EVALUATING THE VON KÁRMÁN CONSTANT IN SEDIMENT-LADEN AIR FLOW

A Dissertation

by

BAILIANG LI

Submitted to the Office of Graduate Studies of
Texas A&M University
in partial fulfillment of the requirements for the degree of

DOCTOR OF PHILOSOPHY

December 2010

Major Subject: Geography

EVALUATING THE VON KÁRMÁN CONSTANT IN SEDIMENT-LADEN AIR FLOW

A Dissertation

by

BAILIANG LI

Submitted to the Office of Graduate Studies of
Texas A&M University
in partial fulfillment of the requirements for the degree of

DOCTOR OF PHILOSOPHY

Approved by:

Chair of Committee,	Douglas J. Sherman
Committee Members,	Vatche P. Tchakerian
	Steven M. Quiring
	Patrick J. Lynett
Head of Department,	Douglas J. Sherman

December 2010

Major Subject: Geography

ABSTRACT

Evaluating the von Kármán Constant in Sediment-laden Air Flow.

(December 2010)

Bailiang Li, B.S., Peking University;

M.S., Chinese Academy of Sciences

Chair of Advisory Committee: Dr. Douglas J. Sherman

Shear velocity is a critical variable used in many hydrodynamic and aeolian applications. The Law of the Wall is commonly used to derive shear velocity as the product of the slope of a measured velocity profile and the von Kármán constant, $\kappa = 0.4$. However, a number of hydrodynamic experiments show that there is a substantial apparent decrease of κ in sediment-laden flow, which was explained by: 1) The energy loss to support the sediment particle suspension in the fluid and 2) The buoyancy effect due to stratification. The energy loss is associated with sediment concentration and grain size, and the stratification can be characterized by sedimentological flux Richardson number or gradient Richardson number. Since there is an apparent change of κ, the term "apparent von Kármán parameter", or κ_a, was adopted from Wright and Parker to replace κ in sediment-laden flow. There has been no study to attempt to detect and to evaluate the variability of κ_a during aeolian saltation, which is the purpose of this dissertation research.

Two "clear air" runs and fifteen "sediment-laden" runs were conducted at the northeast coast of Brazil. Wind profile data were collected by a stack of cup anemometers; "true" shear velocity was estimated by an ultrasonic anemometer; and sediment mass flux profile and grain

size were estimated from the sand samples collected in a stack of vertical hose-style traps. With these estimates, κ_a, sediment concentration and sedimentlogical Richardson numbers were derived.

Regression analysis indicates that there is a statistically insignificant relationship between κ_a and grain size, which may be caused by small range of grain size in the study site. However, there is strong statistical relationship between κ_a and bulk, volumetric concentration below 25 mm, S_{25}, and between κ_a and sediment transport rate Q (kg/m/s) as:

$$\kappa_a = -2088.4 S_{25} + 0.3964 \text{ and } \kappa_a = -3.134 Q + 0.4011$$

A strong relationship was also found between κ_a and sedimentological Richardson numbers in the lower saltation layer, which can be well explained by the stratification theory.

ACKNOWLEDGEMENTS

I would like to thank Prof. Douglas Sherman, my advisor, for his consistent support of my research during my doctoral studies. I am also very thankful to the other committee members: Dr. Vatche Tchakerian, Dr. Steven Quiring, and Dr. Patrick Lynett, for their constructive suggestions on my dissertation.

The field work support was provided from my colleagues: Dr. Jean Ellis, Eugene Farrell, Walter Cox, and also from the staff of LABOMAR, at University of Ceará, especially Professor Luís P. Maia, Paulo H. G. O. Sousa, Robério M. Sampaio, and Eduardo C. M. de Borbaand.

This dissertation research was funded by grants from the Geography and Spatial Sciences Program, National Science Foundation (#0727775 and #0822482). This project is registered with the Brazilian Ministry of the Environment, Sistema de Autorização e Informação em Biodiversidade, Registration Number 18038-1.

Finally, I want to thank Prof. Theodore von Kármán for proposing this apparent constant of 0.4.

NOMENCLATURE

A	a constant of 0.085 during active saltation
D	reference grain diameter of 0.25 mm
H	hose trap opening height (m)
H_s	saltation layer thickness (m)
M	mass flux for each trap (kg)
M_t	total mass flux collected from all traps (kg)
Pr	Prandtl number, defined as v_T/v
Q	sediment transport rate (kg/m/s)
R	hydraulic radius (m)
R_i	sedimentological gradient Richardson number
R_f	sedimentological flux Richardson number
R_{ia}	concentration weighted average R_i
R_{fa}	concentration weighted average R_f
R_{iT}	thermal gradient Richardson number
R_{fT}	thermal flux Richardson number
S	sediment volumetric concentration (m^3/m^3), also as S_v
Sc	Schmidt number, defined as v_s/v
S_g	sediment gravimetric concentration (kg/kg)
S_r	sediment volumetric concentration (m^3/m^3) at z_r
S_v	same as S, volumetric sediment concentration (m^3/m^3)
T	run duration (s)

W	hose trap opening width, here 0.1 m
b	intercept from velocity profile curve fitting, c.f. equation 3-1
c	a constant of 4.2, c.f. equation 2-2
d	mean grain size (mm)
d_{50}	median grain size (mm)
g	gravity acceleration (9.81 m/s^2)
h	water depth (m)
h_c	height of cup anemometer (m)
h_h	height of hose trap stack (m)
h_t	top edge height of each hose trap
h_b	bottom edge height of each hose trap
h_{ua}	height of ultrasonic anemometer
l	mixing length scale (m)
m	slope from velocity profile curve fitting, c.f. equation 3-1
q	normalized sediment mass flux (kg/m/s)
q_{gc}	q at z_{gc} (kg/m/s)
u	time average fluid streamwise velocity (m/s)
u'	instantaneous fluctuation component for u (m/s)
u_*	fluid shear velocity (m/s), derived from the Law of the Wall
u_*'	fluid "true" shear velocity (m/s), derived from Reynolds stress
u_*''	predicted u_*' (m/s) from equation 5-1
u_{*t}	threshold shear velocity (m/s)
v'	instantaneous horizontal fluctuation component normal to u (m/s)

w'	instantaneous vertical fluctuation component (m/s)
w_s	sediment settling velocity (m/s)
z	elevation above surface/bed (m)
z_0	roughens length (m)
z_{0a}	apparent roughens length (m) according to equation 2-4
z_{0s}	modified roughens length (m) according to equation 3-12
z_{gc}	geometric center elevation for each trap (m)
z_r	reference elevation (m)
Φ_m	correction parameter in equation 2-18
α	fitting coefficient in equation 3-8
α_r	empirical constant in equation 2-4
β	fitting coefficient in equation 3-8
θ_T	average potential temperature (K)
θ_T'	instantaneous fluctuation component of θ_T (K)
κ	von Kármán constant in clear fluid, about 0.4
κ_a	apparent von Kármán parameter in stratified fluid
λ	damping coefficient, c.f. equation 2-31
ρ	fluid density, for air, 1.204 kg/m^3
ρ_m	air-sediment mixture density
ρ_s	sediment density, for quartz sand, 2650 kg/ m^3
v	fluid eddy viscosity (m^2/s)
v_T	thermal diffusivity (m^2/s)
v_s	sediment diffusivity (m^2/s)

τ	shear stress (N/m^2), or Reynolds stress
τ_b	shear stress at the bed (N/m^2)

TABLE OF CONTENTS

Page

LIST OF FIGURES

Page

LIST OF TABLES

1. INTRODUCTION

Much of process geomorphology is concerned with understanding the development and evolution of landforms – such as bedforms, channel bars, beaches, or dunes – comprising unconsolidated or poorly consolidated sediments. For example, Ritter et al. (2002, p. 2) define (geomorphic) process "*…as the method by which one thing is produced from something else."* For sedimentary landforms, this method comprises a suite of sub-processes involved in sediment erosion, transport , and deposition, and these processes have been the subject of continued, intense scientific examination for almost a century (early examples include Gilbert, 1914; or Bagnold, 1936). Although sediment transport models have become more sophisticated, especially in terms of the physics involved, it is clear that some models, for a variety of reasons (e.g., Muste, 2002) tend not to produce accurate estimates of transport for natural environments. This is the case for even relatively simple, aeolian transport systems such as large expanses of flat beach (e.g., Sherman et al., 1998).

There are numerous models designed to predict aeolian sediment transport rates, almost all of which depend on the third power of shear velocity (see review by Greeley and Iversen, 1985; Sherman et al., 1998; Shao, 2000; Cornelis and Gabriels, 2003). Shear velocity is also critical in estimating sediment concentration profiles (or Rouse profile, Rouse 1936), and apparent roughness lengths (e.g. Sherman, 1992; Sherman and Farrell, 2008).

In wind tunnel and field experiments, most estimates of shear velocity are derived as the product of the slope of a measured velocity profile and the von Kármán constant, $\kappa = 0.4$. Indirectly, therefore, κ is fundamental for characterizing the sediment transport processes. For

---

This dissertation follows the style of *Annals of American Association of Geographers*.

example, a 10% error in κ would be magnified to an error of about 30% or more in predicted transport rate. However, hydrodynamic research in laboratory flumes indicates that this "constant" may not be constant in the presence of suspended sediments. Indeed values less than 0.2 are reported in the literature (Einstein and Chien, 1955), which would cause 800% errors in transport predictions.

Early hydrodynamic work indicates that the apparent von Kármán constant change can be attributed to the energy loss to support the sediment particles in the fluid. The larger the grain and the greater the concentration, the more energy that is required to keep the grain suspended, leading to a smaller κ (Einstein and Chien, 1955). Therefore, κ is the function of grain size and concentration.

Later water studies (e.g. Adams and Weatherly 1981; Styles and Glenn, 2000) claimed that there is a stratified, density inversion layer, which is similar to the density distribution in the thermally stable atmosphere (lighter/warm air overlays on denser/cool air), where the buoyancy and vertical mixing are damped. This leads to an apparent decrease of κ in the Law of the Wall in the sediment-stratified flow (Wright and Parker, 2004). This apparent change of κ can be modeled by sedimentological Richardson numbers, which quantify the stratification effect in the flow (Styles and Glenn, 2000).

There have been ***no attempts to evaluate the stability/variability of the von Kármán constant in the presence of wind blown sand***. However, the grain concentration in the saltation layer can be substantial during aeolian transport (Ellis et al., 2009). Therefore, the ***purpose of this research is to detect and characterize changes in the von Kármán constant caused by saltation during aeolian sand transport***.

This purpose is formalized in three alternative ***research hypotheses***:

I. The von Kármán constant varies with changes of sand grain size.

II. The von Kármán constant changes as a function of the aeolian mass-flux rate or sediment concentration.

III. The apparent change in the von Kármán constant is caused by flow stratification, or concentration gradient, that can be modeled with a sedimentological version of the Richardson Number.

In order to test these hypotheses, the following ***objectives*** must be accomplished:

I. Identify an appropriate field site, characterized by large, flat, unobstructed sand surfaces with widely varying transport conditions over relatively short time frames.

II. Obtain detailed field measurements of 1) three dimensional wind speed fluctuation components; 2) wind velocity profiles; 3) mass-flux profiles; and 4) sand grain size characteristics.

III. Derive estimates for the von Kármán constant, mean grain size, sediment concentration and the Richardson Number.

IV. Model the von Kármán constant changes in response to changes in mean grain size, sediment concentration, Richardson number and determine the coefficients in the model

V. Determine and assess the uncertainties and potential errors arising from the experiment.

This research on the von Kármán constant in sediment-laden air flow provides an opportunity to evaluate and quantify sediment influences on turbulence from flow stratification. If the von Kármán constant changes with sand transport, this work has the potential to *fundamentally change the interpretation of wind velocity profiles* during saltation and to open debate about the role of sand transport in the alteration of boundary layer processes. If there is a substantial variability in κ, there will be substantial errors in transport rate, flux profile, and roughness length estimates. This means that all aeolian transport studies based on wind profile analysis are flawed to an unknown extent. For environmental managers concerned with beach

and soil protection, dune stabilization, desertification assessment, coastal sediment budgets, and other related environmental challenges, this investigation can lead to improved sediment transport rate models that can provide a sounder basis for rational planning.

2. BACKGROUND

2.1 Importance of the von Kármán constant

Fluid imparts a shear stress on the surface when it moves across it. The shear stress on the surface (or bed) τ_b is often characterized in the form,

$$\tau_b \equiv \rho u_*^2 \qquad (2\text{-}1)$$

where ρ is fluid density, and u_* is shear velocity. In aerodynamic or hydrodynamic studies, u_* has been widely used in many applications, for example:

1) Sediment transport rate prediction. Since the first work of Bagnold (1936), almost all the aeolian transport equations imply Q, the mass transport rate, as a function of u_*^3. Among others, Lettau and Lettau (1977) model illustrates this dependence:

$$Q = c\sqrt{\frac{d}{D}}\frac{\rho}{g}(u_* - u_{*_t})u_*^2 \qquad (2\text{-}2)$$

where u_{*t} is the threshold shear velocity, d is mean grain size in mm, D is reference grain diameter of 0.25 mm, g is gravity acceleration, and c is an empirical constant of 4.2.

2) Sediment concentration profile modeling. Shear velocity is also critical in modeling suspended sediment concentration profile in water. For example, the famous Rouse equation (Rouse, 1936) demonstrates that the concentration profile is controlled by w_s/ u_* as,

$$\frac{S}{S_r} = \left[\frac{z_r(h-z)}{z(h-z_r)}\right]^{\frac{w_s}{Sc\kappa u_*}} \qquad (2\text{-}3)$$

where w_s is sediment settling velocity, S is the volumetric concentration at any elevation z, S_r is the concentration value at reference elevation z_r, and h is water depth, Sc is called Schmidt number (for details, c.f. section 2.4). This equation shows that the slope of the concentration profile is described by the exponent, which is a function of u_*.

3) Apparent roughness length estimation. Roughness length, z_0, derived from Law of the Wall (see below), represents the surface roughness length (or elevation) where velocity equals to zero. During aeolian saltation, z_0 appears much higher than the value without saltation. Many empirical studies indicate that, during aeolian saltation, the apparent roughness length, z_{0a}, is the function of shear velocity. For example, Sherman et al. (1992) proposed

$$z_{0a} = \alpha_r \frac{(u_* - u_{*t})^2}{g} + \frac{2d_{50}}{30} \qquad (2\text{-}4)$$

where α_r is an empirical constant depending on the environmental conditions, d_{50} is the median grain size. Therefore, z_{0a} is proportional to u_*^2.

The accuracy of shear velocity estimation is critical for these applications. In hydrodynamic and aeolian studies, four methods have been commonly employed to obtain shear velocity:

1) Use the Law of the Wall. The Law of the Wall, or the "log law", describes the velocity profile in the boundary layer following a log linear shape as,

$$u(z) = \frac{u_*}{\kappa} \ln(\frac{z}{z_0}) \qquad (2\text{-}5)$$

where $u(z)$ is the mean fluid velocity at elevation z, z_0 is roughness length reflecting the geometric properties of the surface, and κ, called von Kármán constant, is usually treated as a universal constant of about 0.4. The Law of the Wall is the most commonly used equation to obtain shear velocity by measuring the wind profiles in most traditional aeolian experiments (e.g. Bagnold, 1936; Kawamura, 1950; Lettau and Lettau, 1977). For example, if the best fit log-linear slope for equation 2-5 is m, then,

$$u_* = m\kappa \qquad (2\text{-}6)$$

2) Use channel slope S_0 and hydraulic radius R (e.g. Nezu et al., 1997),

$$u_* = \sqrt{gRS_0} \qquad (2\text{-}7)$$

where g is gravitational acceleration. This method can only be used in open channel hydrodynamic studies.

3) Use Reynolds stress (e.g. Nezu et al., 1997),

$$\tau = -\rho\overline{u'w'} = \rho u_*^2(1 - z/h) \qquad (2\text{-}8)$$

where τ is shear stress, or Reynolds stress (c.f. section 2.2), h is fluid depth and u', w' are the instantaneous horizontal and vertical velocity fluctuation components, respectively. This approach is also only viable for hydrodynamic systems. For the air flow, the "log law" assumes that the Reynolds stress does not change much near the bed and is equal to the bed shear stress τ_b (also see the discussion in section 2.2). Therefore,

$$\tau = \tau_b = -\rho\overline{u'w'} = \rho u_*^2 \qquad (2\text{-}9)$$

Thus, the shear velocity can be obtained by measuring the velocity fluctuation components.

4) Direct measurement of τ_b. Equation 2-1 can be rearranged as,

$$u_* \equiv \sqrt{\tau_b / \rho} \qquad (2\text{-}10)$$

Therefore, with known of bed shear stress, the shear velocity can be solved. In aeolian studies, there are some attempts to measure the bed shear stress directly. Several styles of drag meters have been designed, such as floating plate (Sheppard, 1947), ball bearing surface (Kobayashi, 1696), pendulum plate (Bradley, 1968), and load cell plate (Nemoto and Nishimura, 2001; Namikas, 2002). However, these drag plates must be carefully adjusted to the surface to minimize the edge effects (Nemoto and Nishimura, 2001), which may not be appropriate for the long-term deployment in mobile surface. Besides plate-type drag meters, Irwin-type differential pressure sensors have also been used to estimate surface shear stress (Walker and Nicking,

2003). However, the blockage of the sensor opening (1.65 mm of diameter) by flying sand will induce inevitably erroneous measurements, which limits its applicability in the field.

At present, the first method, based on measuring velocity profiles, is still the most commonly used in aeolian studies. From equation 2-6, the shear velocity estimation is not only dependent on velocity profile accuracy, but also the correctness of von Kármán constant. Therefore, if there is a substantial error in the specification of von Kármán constant, all the applications using the shear velocity derived from the Law of the Wall and velocity profiles will be biased.

2.2 Turbulent boundary theory

Although κ is widely known as a constant in the Law of the Wall, the origin of κ is associated with the turbulent boundary theory. Fluid moving across a surface forms a boundary layer due to friction. The upper limit of the boundary layer is usually defined as the elevation at which the flow velocity is 99% of the free stream velocity. In atmospheric science, there are at least two scales of boundary layers. The larger boundary layer is usually called atmospheric boundary layer or planetary boundary layer, which is caused by the contact of the earth surface with troposphere. The thickness of the atmospheric boundary layer can be 100 m at nighttime and 1-2 km at daytime (Oke, 1978, p4). The smaller boundary layer is usually caused by the local surface roughness and convection. The vertical scale may reach 50 m at daytime and shrink to a few meters at nighttime (Oke, 1978, p5). In aeolian studies, the larger one is usually called outer boundary layer, and the smaller one is usually called inner boundary layer (Figure 2-1) or just "boundary layer". This convention is also adopted in this dissertation.

Reynolds number is often used to characterize the flow mode (Reynolds, 1894). Fluid with small Reynolds number usually flows in the form of parallel layers, which is called laminar flow. However, when flow runs faster and Reynolds number is greater than a critical value, the

layers are disrupted, and fluid mixing begins. At this time flow becomes turbulent, which is more effective to transport and mix fluid and momentum (Pope, 2000, p6-7). In a boundary layer with the thickness of the order of 1 to10 m and the mean velocity of the order of 3 to15 m/s and, the flow Reynolds number is 2×10^5 to 10^7, indicating that the air is fully developed turbulent flow. These circumstances are common in most aeolian studies.

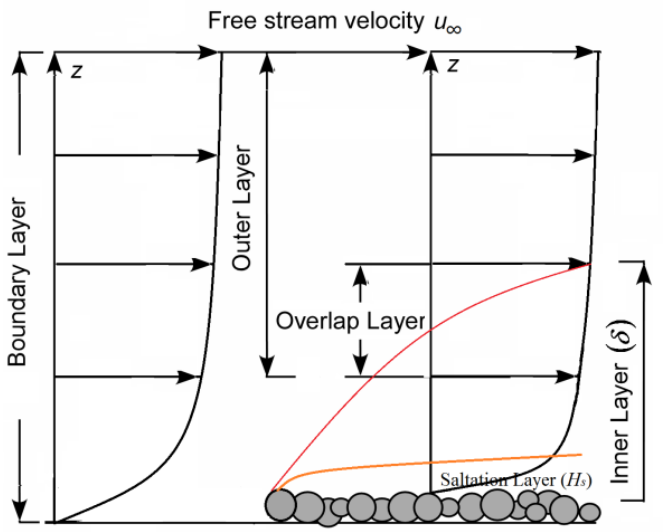

Figure 2-1 Structure of boundary layer (Adapted from Owen and Gillette, 2003 and Middleton and Southard, 1984). Red curve is the upper limit of inner layer. Orange curve is the upper limit of saltation layer. The dimension is not in scale.

Richardson (1922) argued that the turbulence is composed of eddies of different length scales. Later, Prandtl (1925) proposed the concept of mixing length *l* and described the process of fluid mixing inside the turbulent boundary layer. He argued that instead of movement of a single air particle, the typical mixing process can be characterized as the movement of eddies. The average eddy movement length scale is the mixing length *l*. The eddy tends to keep its original characteristics until it finally obtains the local characteristics of the destination. Mixing

length *l* represents the eddy scale of the turbulence fluid, which is similar in each direction. Therefore, mixing length is the function of the instantaneous velocity fluctuations *u′* or *w′*, or

$$w' = u' = l\frac{du}{dz} \tag{2-11}$$

where *du/dz* is the mean velocity gradient.

Von Kármán (1930) proposed a self-similarity theory describing the turbulent mean velocity profile. The theory assumes that the oscillatory attitude of eddies is similar everywhere, while the only difference is time and length scale. If the horizontal velocity at *z+dz* can be expressed as a Taylor series:

$$u(z+dz) = u + \frac{du}{dz}dz + \frac{1}{2}\frac{d^2u}{dz^2}dz^2 + \frac{1}{6}\frac{d^3u}{dz^3}dz^3 + \cdots$$

then according to the similarity theory,

$\frac{du/dz}{d^2u/dz^2} = \frac{l}{\kappa}$, or

$$l = \kappa(du/dz)/(d^2u/dz^2) \tag{2-12}$$

where the scaling parameter κ became known as von Kármán constant. The momentum exchange between fluid layers induces a shear stress, here also called Reynolds stress, which can be expressed as

$$\tau = -\rho\overline{u'w'} \approx \rho\overline{|u'|}\,\overline{|w'|} = \rho l^2\left(\frac{du}{dz}\right)^2 \tag{2-13}$$

After applying Prandtl Mixing Length Theory and Kármán Turbulence Similarity Theory in the turbulent boundary layer near the surface, shear stress near the surface can be treated as a constant and equals bed shear stress τ_b, or

$$\tau = \tau_b = \rho u_*^2 = \rho\kappa^2\frac{(du/dz)^4}{(d^2u/dz^2)^2} \tag{2-14}$$

After resolving the above equation, the Law of the Wall, or "log law" can be obtained as,

$$\frac{du}{dz} = \frac{u_*}{\kappa z} \tag{2-15}$$

It can be also expressed in the form as mentioned in section 2.1:

$$u = \frac{u_*}{\kappa} \ln(\frac{z}{z_0}) \tag{2-16}$$

Law of the Wall also gives the relationship between l and κ in the constant shear layer,

$$l = \kappa z \tag{2-17}$$

During aeolian saltation, there emerges a layer near the surface with a large number of saltating sand grains (below the orange line in Figure 2-1), where the constant shear stress assumption is not valid (Owen, 1964). A number of aeolian experiments (e.g. Bauer et al., 2004; Zhang et al., 2007) have confirmed that within the saltation layer, the Law of the Wall is no longer valid in the saltation layer. Based on the early work of Owen (1964), many studies modeled the velocity profiles within the saltation layer (McEwan, 1993; Werner, 1990; Anderson and Haff, 1991; Shao and Li, 1999; Li et al. 2004). Their results confirmed the experimental results that the wind speed in the saltation layer is faster than that extrapolated from the wind profile line in the constant shear stress layer.

However, even in the constant shear stress layer (i.e. above the saltation layer and within the inner boundary layer), atmospheric scientists found that the validity of the Law of the Wall still depends on the thermal stability of the atmosphere. If the atmosphere is unstable, the buoyancy dominates the air movement. There will be a strong vertical mixing process and the eddy will be stretched (Figure 2-2, b); If the atmosphere is stable, the convection diminishes and the stratified inversion thermal profile (i.e. warm air overlays on cool air) is formed. At this time, the vertical mixing is damped and eddy size will be reduced (Figure 2-2, c). If the air reaches an

equilibrium status, i.e. no vertical mixing damping or enhancement, the air is in the neutral status (Figure 2-2, a). The Law of the Wall is only strictly valid during neutral conditions (Figure 2-2, d), but for the unstable or stable conditions, the Law of the Wall should be modified by a correction parameter Φ_m as (Andreas, et al., 2006),

$$\frac{du}{dz} = \frac{u_*}{\kappa z}\Phi_m \qquad (2\text{-}18)$$

For unstable conditions, $\Phi_m < 1$, and for stable conditions, $\Phi_m > 1$.

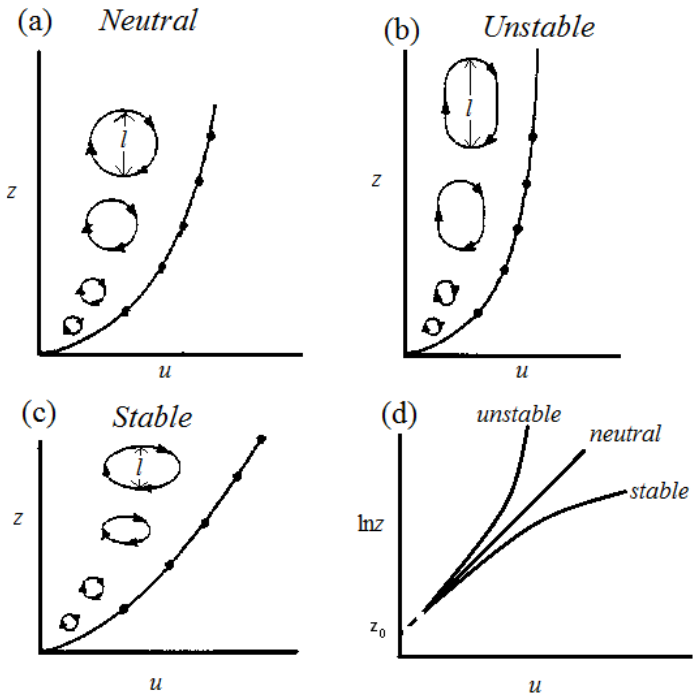

Figure 2-2 Wind velocity profile and eddy structure under different stability conditions (After Oke, 1978, figure 2.9). In (d), y-axis is in logarithmic scale.

The stability of atmosphere is due to the thermal stratification of the flow, which is often quantified by Monin-Obukhov stability parameter (Monin and Obukhov, 1954) or thermal Richardson number (Lettau and Davidson, 1957). For the latter, it is often expressed as in two

forms, thermal flux Richardson number, R_{fT}, and thermal gradient Richardson number, R_{iT} (e.g. Pardyjak, et al., 2002).

For flux Richardson number, it can be defined as (e.g. Stull, 1988, p 175),

$$R_{fT} = \frac{-g/\theta_T \cdot \overline{\theta_T' w'}}{\overline{u'w'}(du/dz)} \qquad (2\text{-}19)$$

where θ_T is mean potential temperature at z and θ_T' is the instantaneous potential temperature fluctuation component. Thermal flux Richardson number is the ratio of buoyancy production term to turbulent production term. For thermal gradient Richardson number, can be defined in the form as (e.g. Brunel, 1989),

$$R_{iT} = \frac{-g/\theta_T \cdot d\theta_T/dz}{(du/dz)^2} \qquad (2\text{-}20)$$

R_{iT} also measures the relative importance of buoyancy versus mechanical forces in the boundary layer. When R_{fT} and R_{iT} are greater than 0, buoyancy effect begins to damp the vertical mixing and reduce the eddy size, and the flow becomes stably stratified; when R_{fT} and R_{iT} reach a critical value of about 0.25, turbulence production stops, eddies disappear and the flow becomes laminar (c.f. Howard, 1961; Thom, 1975; Stull, 1976, p176). If rearranging the above two equations, the relationship between R_{fT} and R_{iT} can be expressed as a function of Prandtl number Pr as,

$$\frac{R_{fT}}{R_{iT}} = \frac{\overline{\theta_T' w'}}{d\theta_T/dz} \Big/ \frac{\overline{u'w'}}{du/dz} = \frac{\upsilon_T}{\upsilon} = \Pr \qquad (2\text{-}21)$$

$$\text{or } R_{fT} = \Pr R_{iT} \qquad (2\text{-}22)$$

where Pr is defined as the ratio of thermal diffusivity v_T to air eddy viscosity v.

Since thermal Richardson numbers can be used to represent the stratification effect of the flow, the correction factor Φ_m in modified Law of the Wall can be linked with these Richardson numbers. For stably stratified flow, there is an inversed linear relationship between

Φ_m and thermal Richardson numbers as (e.g. Businger et al., 1971):

$$\Phi_m = \frac{1}{1-\lambda R_{fT}} = \frac{1}{1-\Pr \lambda R_{iT}} \qquad (2\text{-}23)$$

where λ is the damping coefficient. Businger et al. (1971) based on an extensive experiment on atmospheric boundary layer and concluded that *Pr*= 1.35 and λ = 4.7. A later study (Högström, 1988) corrected some experimental errors cited by Businger et al. (1971) and addressed a pair of new values of *Pr* and λ as 1.05 and 5.71. The new *Pr* value explains the reason why the critical values for these Richardson numbers are very close.

On the other hand, the correction of Law of the Wall may be also accomplished as the eddy scale change (c.f. Figure 2-2), or the change of von Kármán constant, i.e.,

$$\frac{du}{dz} = \frac{u_*}{\kappa z}\Phi_m = \frac{u_*}{\kappa(\Phi_m)z} \qquad (2\text{-}24)$$

with $$\kappa(\Phi_m) = \frac{\kappa}{\Phi_m} \qquad (2\text{-}25)$$

To iterate, the Law of the Wall is only strictly valid under neutral conditions, for thermally stratified flow, there will be an apparent change of κ, which is the function of the correction factor Φ_m.

2.3 The variability of von Kármán constant

For clear fluids (i.e. the sediment influence on the fluid can be ignored), many studies in the water pipes (e.g. Nikuradse, 1932), channels (e.g. Keulegan, 1938), and atmospheric surface layer (e.g. Frenzen and Vogel, 1995a, b) found that the von Kármán constant varies in the limited range of 0.36-0.43 under neutral conditions. A recent atmospheric experiment over polar sea ice confirmed κ within the range of 0.387 ± 0.003 after Φ_m correction (Andreas et al., 2006). These results suggest that although there remains some uncertainty of the exact value of κ, it

does lie quite near 0.40, the value commonly assumed in studies of blowing sand (e.g. Bagnold, 1936; Kawamura, 1951).

However, studies on sediment-laden fluids indicate that although the "log law" is still valid in the inner turbulent region, the von Kármán constant variability can be substantial. The following table (Table 2-1) summarizes several experiments of flumes and rivers.

Table 2-1 Summaries of main parameters from selected former experiments

Experiments	κ range	Maximum Sediment Concentration (kg/m^3)	Median grain size (D_{50}) range (mm)	particle density (kg/m^3)
Kalinske and Hsia, 1945	0.32-0.44	118.1 (Uniform concentration)	0.011	2670
Einstein and Chien, 1955	0.173-0.403	328 (z/h=0.0645)	1.30	2650
	0.247-0.410	263 (z/h=0.0403)	0.94	
	0.168-0.406	625 (z/h=0.0393)	0.274	
Vanoni and Nomicos, 1960	0.209-0.384	8.08 (Unspecified height)	0.105 (mean grain size)	2650
	0.299-0.364	3.61 (Unspecified height)	0.161 (mean grain size)	2650
Elata and Ippen, 1961	0.248-0.387	279.3 (Uniform concentration)	85% sand diameter with 0.1-0.155mm	1050
Coleman,1981, 1986	Mean=0.392 Sd=0.0085	198.75 (Extrapolated conc. at bed)	0.105	Quartz and feldspar (About 2650)
	Mean=0.422 Sd=0.0160	188.15 (Extrapolated conc. at bed)	0.210	
	Mean=0.401 Sd=0.0226	265.0 (Extrapolated conc. at bed)	0.420	
Gust and Southard, 1983	0.28	3.3×10-3+30% g /m/s (bed load)	0.16	2320
Nouh, 1989	0.315-0.465 (straight flume)	26.11 (vertical mean)	0.03	2650
Wang and Larsen, 1994	0.38 (Suspended load only)	279.0 (Uniformly distributed)	0.004	2680
	0.16 (Bed load and suspended load)	279.0 (Suspended load) Bed load transport rate = 8.80 kg/m/s	0.004 (Suspended load) 1.5 (Bed load)	2680 (Suspended load) 2640 (Bed load)
Best et al. 1997	0.390-0.413	0.6474 (Unspecified height)	0.22	2600

Table 2-1 Continued

Experiments	κ range	Maximum Sediment Concentration (kg/m^3)	Median grain size (D_{50}) range (mm)	particle density (kg/m^3)
Bennett et al. 1998	0.28-0.34	Approx. 238.5 (z/h=0.00667)	Mean = 0.256 Std = 1.185	2650
Nezu and Azuma 2004	0.400	0.315 (Vertical mean)	0.3	1050
	0.399	0.84 (Vertical mean)	0.5	
	0.397	1.155 (Vertical mean)	0.8	
	0.396	1.365 (Vertical mean)	1.0	
	0.394	3.36 (Vertical mean)	1.3	
Wright and Parker 2004	0.94 κ	0.86 (Discharge weighted mean)	0.25-0.31	Natural river sediment
	0.84 κ	2.100 (Discharge weighted mean)	0.2-0.42	
	0.80 κ	1.730 (Discharge weighted mean)	0.15-0.39	
	0.67 κ	0.600 (Discharge weighted mean)	0.10-0.22	
	0.63 κ	0.360 (Discharge weighted mean)	0.09-0.29	
	0.64 κ	0.230 (Discharge weighted mean)	0.18-0.32	

Note: κ in Wright and Parker (2004) refers to the von Kármán constant value in the clear flow

Table 2-1shows that the influence of the sediment concentration to the von Kármán constant is controversial; some studies show that the sediment has little influence on κ (e.g. Coleman, 1986; Keulegan, 1938), but most of them concluded that the greater the sediment concentration, the smaller the von Kármán constant (Einstein and Chien, 1955; Vanoni and Nomicos, 1960; Elata and Ippen, 1961; Best et al., 1997; Bennett et al., 1998; Nezu and Azuma, 2004). The value of κ could be as small as 0.168 according to the above literature, which is much lower than the range measured in the clear fluid. Therefore, the potential impact from assuming constant of κ cannot be neglected, especially when the sediment concentration is very high.

There has been no analogous research on the influence of aeolian sediment concentration on the von Kármán constant, but the variability of κ could be substantial in sediment-laden air flow. For example, assume a flat sand sheet with roughness length of 0.2 mm, and a wind shear

velocity of 0.5 m/s. According the Law of the Wall (suppose that $\kappa = 0.4$), the velocity at 0.1 m will be about 7.8 m/s, and 6.9 m/s at 0.05 m. Following the well-known Bagnold's sediment transport equation (Bagnold, 1936), the total sediment transport rate is about 0.03 kg/m/s. In the case that about 85% of total sediment flux occurs below 0.1 m, and about 62% below 0.05 m (e.g. Namikas, 2003), the mean sediment concentration could reach about 0.06 kg/m^3 (0.05 m) and 0.05 kg/m^3 (0.1 m). Compared to the experiments in Table 2-1, it is easy to see there is more than three orders of magnitude difference of sediment concentrations between water and air. However, there are also three orders of magnitude difference in fluid densities. Therefore, the mean gravimetric sediment concentration in the air (0.05 kg/kg below 0.05 m or 0.04 kg/kg below 0.1 m), is comparable to the sediment concentration in water (e.g. 0.026 kg/kg, or 26.11kg/m^3 from Nouh, 1989). Similar variability of κ is expected to occur in the sediment-laden air flow.

Table 2-1 also indicates that sediment concentration may not be only one factor to control the variability of κ. For example, Wright and Parker (2004) reported several smaller κ values with smaller sediment concentrations but larger grain sizes, which show grain size may be also an important factor to cause κ variation. Therefore, one of objectives of this study is to examine if the grain size is correlated to the variability of κ.

2.4 Explanations of the variability of κ

The variability of κ with the changes of concentration and grain size was explained by the "supporting energy" theory. Supporting energy is the energy the fluid needs to keep the sediment particles suspended. Einstein and Chien (1955) and Vanoni and Nomicos (1960) proposed two different but related parameters to illustrate the importance of the grain size and sediment concentration, they argued that the larger the grain size (or the settling velocity, v_{si} in

Figure 2-3) or the greater the sediment concentration (C_i in Figure 2-3), the greater the energy needed to support the suspension of the grains. This leads to the reduction of eddy size, hence κ.

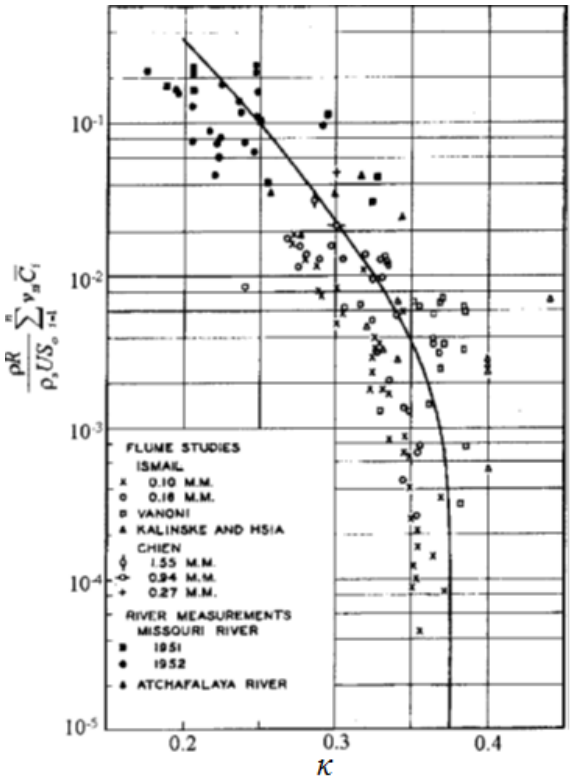

Figure 2-3 Empirical correlation between κ and a supporting energy parameter (Einstein and Chien 1955).

Also from an energy perspective, Barton and Lin (1955) argued that, compared to clear flow, the sediment-laden flow requires extra energy to overcome the buoyancy effect due to density stratification, which can be interpreted using the Richardson number concept. In analogy to thermal gradient Richardson number, the sedimentological gradient Richardson number (R_i) is defined as (e.g. Chien and Wan, 1999):

$$R_i = \frac{-g/\rho_m \cdot d\rho_m/dz}{(du/dz)^2} \qquad (2\text{-}26)$$

where ρ_m is the fluid-sediment mixture density. R_i represents the sedimentological stratification effect due to mixture density gradient, which is similar to stably thermal stratification in the atmospheric boundary layer, where dense (cold) air is lower than light (warm) air. Under such conditions, the vertical mixing is damped and the eddy size is reduced. Therefore, as the scaling coefficient of eddy size, κ would decrease with increase of density gradient.

Equation 2-26 indicates that R_i is the function of elevation z, and the vertical average R_i was later found to be equivalent to the supporting energy parameters proposed by Einstein and Chien (1955) and Vanoni and Nomicos (1960), and there is a negative relationship between the vertical average Ri and κ in the flow with suspended sediment (Chien and Wan, 1999). However, for the flow with sediment concentrated near the bed, the local R_i near the bed has stronger relationship with κ than the vertical average R_i does (Chien and Wan, 1999).

Aeolian saltation forms a saltation layer near the bed. The thickness of the layer is the function of shear velocity (Owen, 1980) or sediment flux profile (Li et al., 2004). Since the vertical sediment flux distribution is usually exponential (Ellis, et al., 2009), a substantial density gradient is expected in the saltation layer, indicating the stratification effect in that layer cannot be neglected. Therefore, there should be a significant relationship between κ and local R_i near the bed.

Adams and Weatherly (1981) argued that the failure to account for the stratification due to presence of sediment in the fluid can lead to overestimation of shear velocity when using the Law of the Wall. Instead of adopting the stratification correction parameter Φ_m, Wright and Parker (2004) proposed the concept of apparent von Kármán parameter, κ_a to account for the

velocity profile change due to the sedimentological stratification. Based on this concept, they modified the Law of the Wall as,

$$\frac{1}{\kappa_a} = \frac{d\left(u/u_*'\right)}{d\left(\ln z\right)} = \frac{z}{u_*'}\frac{du}{dz} \qquad (2\text{-}27)$$

where u_*' is the "true" shear velocity, different from the shear velocity derived from the Law of the Wall and velocity profiles. Then stratification correction parameter Φ_m has the following relationship with κ_a,

$$\kappa_a = \kappa / \Phi_m \qquad (2\text{-}28)$$

From the discussion on thermally stratified flow, the value of κ_a or Φ_m should be the function of the Richardson numbers. The sedimentological flux Richardson number, R_f, is defined as (e.g. Syles and Glenn, 2000):

$$R_f = \frac{-g/\rho_m \overline{\rho_m' w'}}{\overline{u'w'}\partial u/\partial z} \qquad (2\text{-}29)$$

Similarly to equation 2-22, the relationship between R_f, and R_i is expressed as (c.f. Glenn and Grant, 1987; Styles and Glenn, 2000; Hermmann and Madsen, 2007)

$$R_f = ScR_i \qquad (2\text{-}30)$$

where Sc, Schmidt number, different from Prandtl number, is the ratio of the sediment eddy diffusivity(v_S) to eddy viscosity (v). In analogy to thermally stratified flow, the relationship between correction parameters (κ_a and Φ_m) and Richardson numbers (R_i and R_f) in sediment-stratified flow can be described as (Smith and Mclean, 1977):

$$\Phi_m = \frac{\kappa}{\kappa_a} = \frac{1}{1-\lambda R_f} = \frac{1}{1-Sc\lambda R_i} \qquad (2\text{-}31)$$

where λ is the damping coefficient. Gelfenbaum and Smith (1986), after analyzing the experiments by Vanoni and Einstein and Chien, argued that $\lambda = 6.9$ is valid in the weakly

stratified flow, and 10.0 for strongly stratified flow. For *Sc*, disparate values had been proposed in sediment laden water flow, e.g., $1 < Sc < 10$ by Lees (1981), from less than 1 to more than 1 by van Rijn (1985), $0.1 < Sc < 0.5$ by Farber (1986), 0.2 by Soulsby et al. (1986), and $0.90 < Sc < 2.38$ by Rose and Thorne (2001). Graf and Cellino (2002) argued that $Sc > 1$ for surface with bed forms, and $Sc < 1$ for flat surface. Most recently, Hermmann and Madsen (2007) suggested $Sc = 0.8$ and $\lambda = 4.0$.

2.5 Summary

The Law of the Wall is not valid in the sediment-stratified flow, which can be corrected using apparent von Kárman parameter κ_a or stratification parameter Φ_m. Since profound density gradient also exists during aeolian saltation, the apparent von Kárman parameter change is expected in the sediment-laden air flow. To evaluate the possible variability of κ_a using equation 2-27, there must be an independent estimate of shear velocity. Here the Reynolds stress method was adopted.

3. STUDY SITE AND METHODOLOGY

3.1 Study site location

The success of this project depends to a large extent on the selection of the study site. Desirable attributes for the site included a reliable (for sand transport) wind regime, minimal rainfall, large expanses of relatively flat and unobstructed sand surfaces, and access to support facilities in case of instrumentation problems. My field experiment was conducted at two sites at the state of Cear á, northeastern Brazil, in the vicinity of Jericoacoara (Figure 3-1).

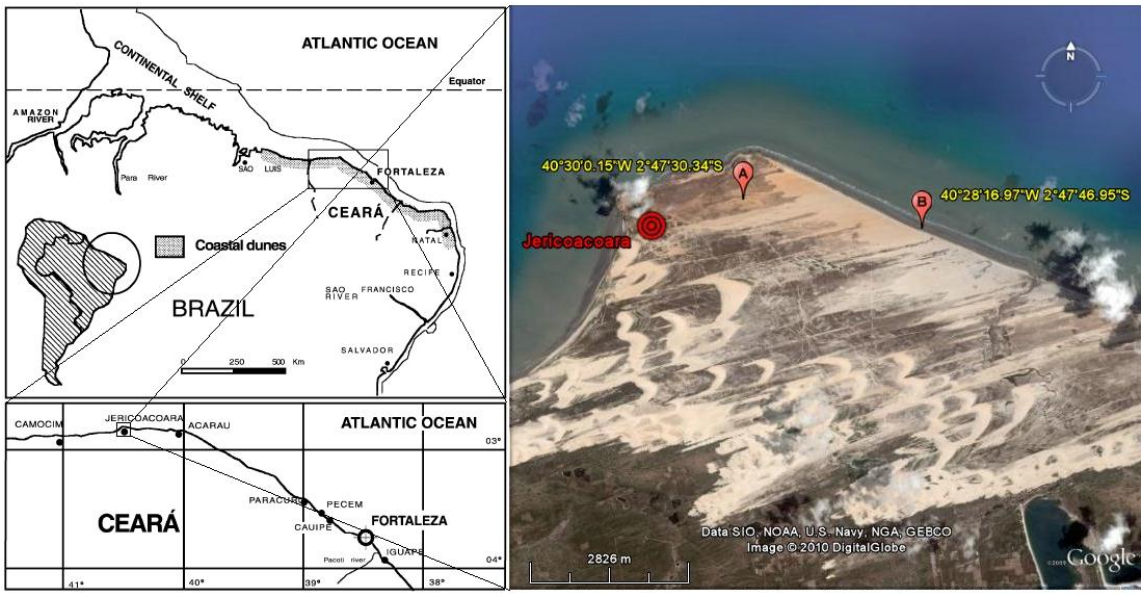

Figure 3-1 Study sites near Jericoacoara (Adapted from Jeminez et al., 1999; Google Earth, 2010).

The first site was located in the middle of depression of a blown-out, parabolic dune near the center of the foreland (A in Figure 3-1, 40º30′0.15″W 2º47′30.34″S). The wind at this site was oriented by the relic ridges of the parabolic dune and remained almost unidirectional. The study site has the fetch length to the instrument location over 100 m (Figure 3-2), with the

distance between the ridges about 50 m. Fifteen runs of sediment-laden air studies were conducted at this site.

Figure 3-2 Study site A. Picture was taken upwind.

The second site was located on an inter-tidal, wet, sand flat on the eastern (upwind) side of the foreland (B in Figure 3-1, 40º28′16.97″W 2º47′46.95″S). It has unobstructed fetch length of over 200 m (Figure 3-3), and the wet sands remained immobile even with the wind speed over 10 m/s. Two "clear air" runs were conducted at this site on Nov 1, 2008.

The study sites have a Savanna climate according to Köppen climate system, with average precipitation smaller than 50 mm and prevailing ESE wind of about 8 m/s from August to November (Maia et al., 2005). The field experiment was conducted in October and November, 2008. No rainfall was recorded during the stay in Jericoacoara.

Figure 3-3 Study site B. Picture was taken downwind.

3.2 Instrumentation

In order to test the hypotheses, the following variables are required to be measured: at one elevation, vertical and horizontal velocity fluctuations (for shear stress in equation 2-9); at multiple elevations, instantaneous horizontal velocity (for velocity profile slope); and the vertical sediment flux profile (for sediment transport rate, sediment concentration and grain size distribution) over a period of time.

3.2.1 Anemometers

The velocity fluctuation components (u', v' and w') were measured with an ultrasonic anemometer (RM Young 81000) (Figure 3-4, left), with an internal sampling rate of 160 Hz and 32 Hz output rate). This type of anemometer can measure the 3-D instantaneous velocities by six ultrasonic sensors (black bars in Figure 3-4, left), protected by three steel frames. Van Boxel et

al. (2004) suggested using sampling rate at least 20 Hz for an instrument located at 1 m elevation if the wind velocity is of the order of 10m/s. For these conditions, the sampling duration should be at least 2 minutes to keep the variance losses of Reynolds stress less than 5%. If the height is too low, the required sampling rate will increase significantly, and if too high, then it would take longer time to minimize the loss of Reynolds stress. Therefore, the instrument was mounted at an elevation where measurements were centered at 1 m above the bed, the output sampling rate was set at 32 Hz, and the sampling duration lasted at least 2 minutes. The measurements obtained allowed equation 2-27 to be solved for "true" shear velocity u_*'.

Wind speed at multiple elevations was measured with a vertical array of four Gill type, 3-cup anemometers (Figure 3-4, left). These velocity profile measurements, together with u_*' obtained above, helped to find the apparent von Kármán parameter according to Law of the Wall.

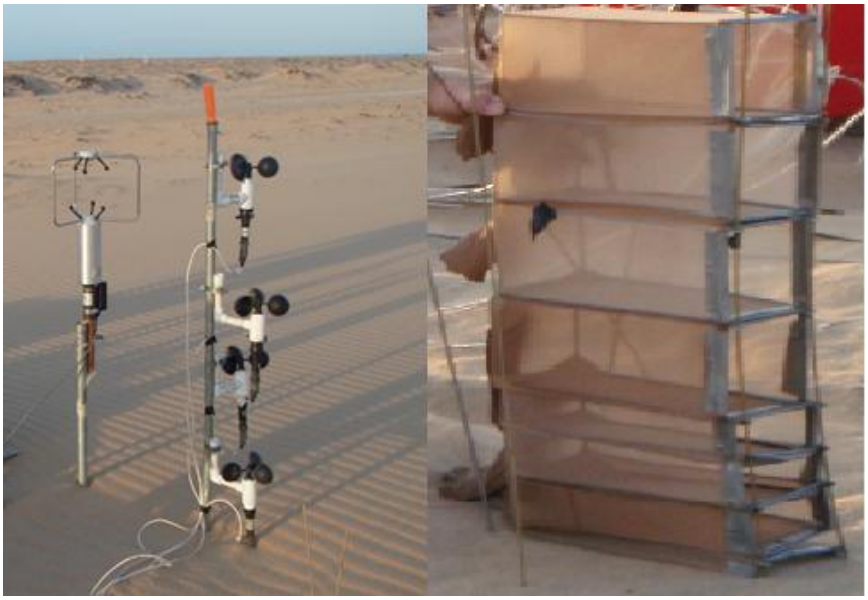

Figure 3-4 Instruments used in the experiment. Left: ultrasonic anemometer and cup anemometers; Right: hose traps.

3.2.2 Hose traps

Hose-style sand traps (Pease et al., 2002) were used here for two purposes: 1) measuring the sediment transport rate, 2) obtaining samples for grain size analysis. The hose traps are 0.2 m long and 0.1 m wide, their height has three dimensions: 0.1 m, 0.05 m or 0.025 m (Figure 3-4, right). During the experiment, smaller traps were deployed closer to the surface to catch more detail distribution of vertical mass flux profile.

3.3 Instrument deployment

3.3.1 Instrument configuration

The configuration of the instrument array at Site A is depicted in Figure 3-5. One ultrasonic anemometer is located at 1.0 m (c.f. h_{ua} in Table 3-1) above bed to measure Reynolds stress, four cup anemometers deployed at elevations of 0.25, 0.5, 0.75 and 1.0 m (for certain runs, one cup anemometer failed to collect data, c.f. h_c in Table 3-1) to measure the wind velocity profile. A stack of 8 hose traps were deployed about 0.5 m from cup anemometer array. There are two 0.025 m-height traps at the bottom and three 0.05 m traps in the middle and three 0.1 m traps stacked on the top. The height of the trap stack is 0.555 m (c.f. h_h in Table 3-1). We have conducted 15 runs in the study site A (Run 1 to 15 in Table 3-1). Each run has the duration T from 120s to 300s. In order to obtain the von Kármán constant in the clear air flow, 2 runs were conducted at study site B. The only difference of the instrument configuration from sediment-laden experiment is the removal of hose traps. The detailed settings of these two runs are also listed in Table 3-1.

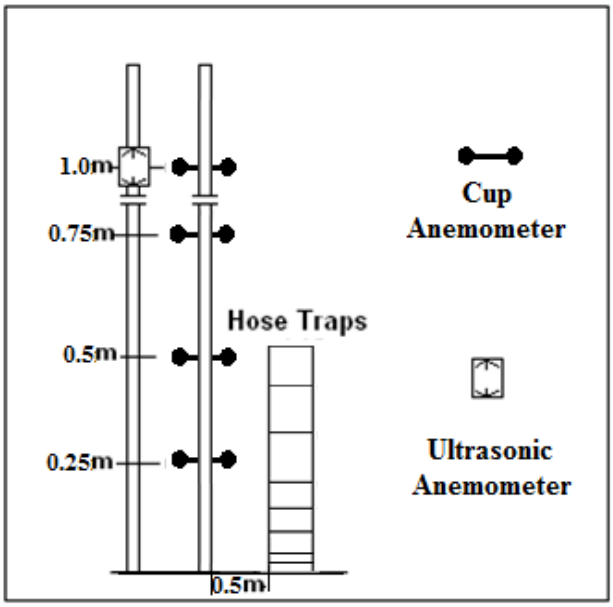

Figure 3-5 Instrument configuration during experiment with sand transport (Run 1-15, Site B).

Table 3-1 Experiment settings for all runs. (Run 1-15 at Site B, Run 16-17 at Site A)

Run	Date	T (s)	h_{ua} (m)	h_h (m)	h_c (m)			
1	10/22	120	1	0.555	0.25	0.5	0.75	1
2	10/22	180	1	0.555	0.25	0.5	0.75	1
3	10/22	180	1	0.555	0.25	0.5	0.75	1
4	10/22	213	1	0.555	0.25	0.5	0.75	1
5	10/24	170	1	0.555	0.25	0.5	0.75	1
6	10/24	240	1	0.555	0.25	0.5	0.75	1
7	10/24	240	1	0.555	0.25	0.5	0.75	1
8	10/24	240	1	0.555	0.25	0.5	0.75	1
9	10/24	240	1	0.555	0.25	0.5	0.75	1
10	10/24	240	1	0.555	0.25	0.5	0.75	1
11	10/26	240	1	0.555	0.25	0.5	0.75	1
12	10/26	300	1	0.555	0.25	0.5	0.75	1
13	10/30	240	1	0.555	0.25	0.5	-	1
14	10/30	299	1	0.555	0.25	0.5	-	1
15	10/30	240	1	0.555	0.25	0.5	-	1
16	11/1	612	1	-	0.25	0.5	-	1
17	11/1	644	1	-	0.25	0.5	-	1

3.3.2 Data acquisition

All electronic instruments were hard-wired to a laptop-based data acquisition system (National Instruments 9250) with 32 analog input channels. All the instruments were synchronized at 96 Hz sampling rate, ultrasonic anemometer data were subsampled to 32 Hz, and cup anemometer data were subsampled to 4 Hz.

3.4 Signal processing

3.4.1 Instrument recalibration

The manufacturer's calibration data for the ultrasonic anemometers were not valid due to the voltage loss through the cables used in the field. We recalibrated those sensors with and without cable extensions in the Oran W. Nicks Low Speed Wind Tunnel located on Texas A&M University campus. The test section has the dimension of 3.66 m $\times$ 3.05 m $\times$ 2.13 m. The wind tunnel can provide steady wind velocity up to 85 m/s, with the accuracy controlled within $\pm$0.01 m/s. We obtained the calibrated data corresponding to wind velocities from 5 m/s to 20 m/s at 2.5 m/s increment of speed, and the new calibrations have the R^2 of 1.00.

3.4.2 Cup anemometers

Data (in v) from the cup anemometers were subsampled to 4 Hz by selecting a median value for every 24-point block to avoid the occasional spike (e.g. Figure 3-6). If spikes still exist after subsampling, those spikes were linearly interpolated by the neighbor values. Subsampled signals (in v) from cup anemometers were converted to velocity (m/s) by factory calibrations.

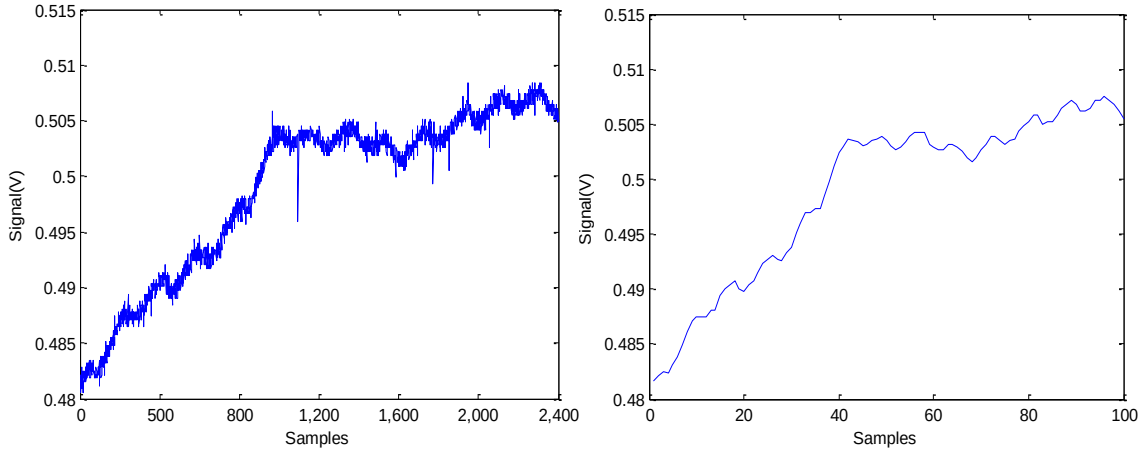

Figure 3-6 Data reduction for cup anemometer measurements. Left: before subsampling. Right: after subsampling.

3.4.3 Ultrasonic anemometers

Ultrasonic anemometers data were subsampled to 32 Hz from the original time series by adopting the similar method for the cup anemometer (using 3-point block). The subsampled data (in v) were converted into velocity (in m/s) using the calibrations from the wind tunnel experiment.

Reynolds stress estimates require measuring velocity fluctuation components u', v' and w'. In order to correctly obtain those values, the 3-D velocities require three steps of rotation (c.f. Kaimal and Finnigan, 1994; van Boxel et al., 2004):

1) If the original instantaneous velocities are u_0, v_0 and w_0 (Figure 3-7, left), the transformed velocities are u_1, v_1 and w_1, this rotation is to orient u_0 to the wind direction and also make the mean transverse component $\overline{v_1}$ become zero, i.e.

$$u_1 = u_0 \cos\theta + v_0 \sin\theta$$
$$v_1 = -u_0 \sin\theta + v_0 \cos\theta$$
$$w_1 = w_0$$
$$\theta = \arctan(\overline{v_0} / \overline{u_0})$$

2) The second rotation is to make the u_1 aligned to the sloping streamlines and w_1 perpendicular to the streamlines, or after rotation, $\overline{w_2} = 0$:

$$u_2 = u_1 \cos\Phi + w_1 \sin\Phi$$
$$v_2 = v_1$$
$$w_2 = -u_1 \sin\Phi + w_1 \cos\Phi$$
$$\Phi = \arctan(\overline{w_1} / \overline{u_1})$$

3) The last rotation is to orient v_2 to the stream surface and w_2 normal to the surface, or after rotation, $\overline{v_3' w_3'} = 0$:

$$u_3 = u_2$$
$$v_3 = v_2 \cos\Psi + w_2 \sin\Psi$$
$$w_3 = -u_2 \sin\Psi + w_{21} \cos\Psi$$
$$\Psi = \arctan\left(\frac{2\overline{v_2 w_2}}{\overline{v_2^2} - \overline{w_2^2}} \right)$$

After rotation (Figure 3-7, right), the 3-D velocity fluctuation components *u'*, *v'* and *w*' can be calculated by subtracting the mean speeds from their instantaneous values.

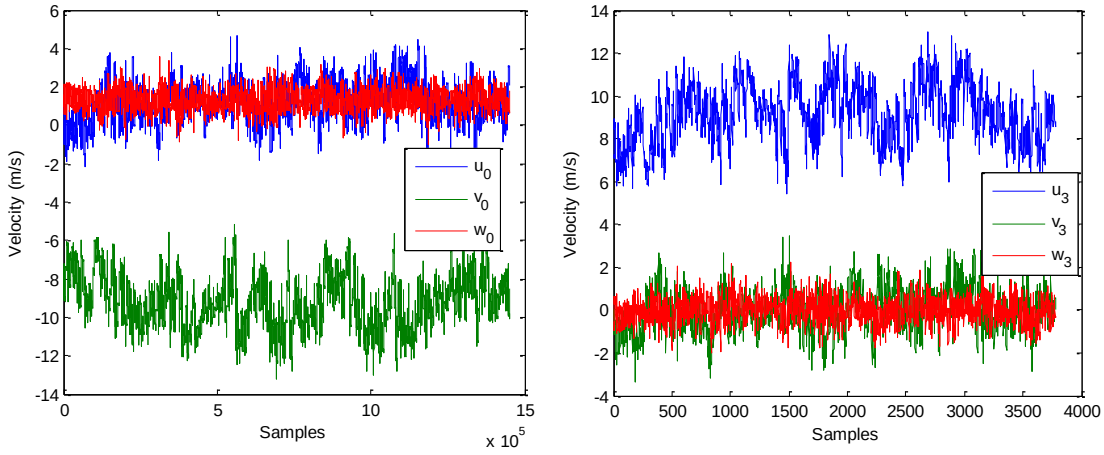

Figure 3-7 Ultrasonic anemometer measurements before (left) and after (right) rotation. Before rotation, the maximum velocity is negative *y* direction because the *v* channel of ultrasonic anemometer was oriented facing the wind to avoid the influence from the steel frames.

3.5 Variable derivation

In order to test hypotheses, mean grain size, apparent von Kármán parameter, sediment transport rate, sediment concentration, and sedimentological Richardson number must be derived.

3.5.1 Mean grain size *d*

Sediment samples collected from the hose traps were weighted and split in the field, and the subsamples were transported to laboratory and then dry-sieved at 0.25 φ intervals using a commercial sonic sifter separator (ATM Corp. Model L3P). The mean grain size for each sample was computed using MS Excel-based software, *GRADISTAT* (Blott and Pye, 2001). The mean grain size *d* for a certain run was calculated by weighted averaging the mean grain size from all the traps deployed.

3.5.2 Apparent von Kármán parameter κ_a

Cup anemometers give the streamline velocities at multiple elevations. As mentioned in section 2.1, in most traditional aeolian studies, shear velocity is calculated from the Law of the Wall by fitting the log- linear regression line between *u* and *z* using the following equation:

$$u = m\log(z) + b \qquad (3\text{-}1)$$

here, *m* is the slope of the least-square line, and *b* is the intercept. The uncorrected shear velocity can be calculated by the assumption of $\kappa = 0.4$ (e.g. Bagnold, 1936; Kawamura, 1951).

$$u_* = m\kappa = 0.4m \qquad (3\text{-}2)$$

The apparent roughness length can be estimated by:

$$z_{0a} = \exp(-b/m) \qquad (3\text{-}3)$$

Here the calculated shear velocity u_* is different from the "true" shear velocity from the Reynolds stress method u_*'. As described in section 2.1, u_*' can be calculated from the following equation:

$$u_*' = \sqrt{-u'w'} \quad (3\text{-}4)$$

According to equation 2-27, the apparent von Kármán parameter κ_a can calculated from m and u_*',

$$\kappa_a = u_*' / m \quad (3\text{-}5)$$

3.5.3 Sediment transport rate Q and normalized sediment flux q

The sediment transport rate, Q (kg/m/s) can be obtained after normalizing the total sediment flux, M_t (kg) by trap width, W (m), and run duration, T (s),

$$Q = \frac{M_t}{WT} \quad (3\text{-}6)$$

If the mass flux from each trap is M (kg), the normalized sediment mass flux q (kg/m^2/s) for each trap can be calculated by

$$q = \frac{M}{WHT} \quad (3\text{-}7)$$

where H is the opening height of the hose trap (m).

As described by Ellis et al. (2009), the mass flux profile can be described quantitatively by fitting an exponential curve between geometric center elevation and normalized sediment mass flux of each trap, or

$$q = \alpha \exp(\beta z_{gc}) \quad (3\text{-}8)$$

where, α and β are fitting coefficients, and z_{gc} is geometric center elevation for each trap. During calculating z_{gc}, the lower edge of the bottom trap was set at z_0. The normalized mass flux profile was used to calculate sediment concentration and sedimentological Richardson number.

3.5.4 Sediment concentration S

Sediment concentration can be represented as in gravimetric S_g (sediment mass/mixture mass, in kg/kg) or volumetric S_v (sediment volume/mixture volume, in m^3/m^3),

$$S_g = \frac{M}{\rho V + M} \tag{3-9}$$

$$S_v = \frac{M/\rho_s}{V + M/\rho_s} = \frac{M}{\rho_s V + M} \tag{3-10}$$

where ρ_s is the sediment density (for quartz sand, it is about 2650 kg/m^3) and V is the volume (m^3) of air passing through the hose trap, which can be obtained by integrate the wind velocity profile, or

$$V = WT\int_{h_b}^{h_t} u dz \tag{3-11}$$

where h_t and h_b are the top and bottom edge elevations of the trap, respectively.

The velocity profile outside saltation layer can be estimated from equation 3-1. The velocity profile within the saltation layer can be estimated using the model proposed by Li et al. (2004). The reason to choose this model is because it is verified by experimental data, and its analytical form is more easily applied. Following Li et al. (2004), the wind speed in the saltation layer can be expressed as,

$$u = m\int_{z_{0s}}^{z} \frac{1}{z}\sqrt{1-(1-\frac{u_{*t}^2}{(u_*^{'})^2})(1-\frac{z}{H_s})e^{\beta z}}\, dz \tag{3-12}$$

where z_{0s} is the modified roughness length, which can be determined by matching the modified profile with log profile at saltation layer height, H_s, defined as the mean maximum height of sand grain saltation, where β is the slope of the sediment flux profile from equation 3-8, and u_{*t}, the threshold shear velocity, is usually estimated by Bagnold's (1936) equation as,

$$u_{*t} = A\sqrt{gd(\frac{\rho_s - \rho}{\rho})} \tag{3-13}$$

where A is a constant equal to 0.085 during conditions of active saltation. As mentioned in section 2.4, the saltation layer thickness can be estimated by two methods

1) Owen, 1980

$$H_s = 0.82(u_*^{'})^2 / g \quad (3\text{-}14)$$

2) Li et al., 2004

$$H_s = -1/\beta \quad (3\text{-}15)$$

Both methods were used in this study for comparison purposes.

Velocity can be considered as the amount of volume of air passing through a unit of cross-section area per unit of time, therefore, volumetric concentration profile can be also estimated by normalized flux profile and velocity profile as

$$S_v = \frac{q/\rho_s}{q/\rho_s + u} \quad (3\text{-}16)$$

3.5.5 Sediment-air mixture density ρ_m

In order to obtain density based Richardson number, air-sediment mixture density should be computed first, defined as total mixture mass divided by total mixture volume,

$$\rho_m = \frac{M + \rho V}{M/\rho_s + V} \quad (3\text{-}17)$$

The air-sediment mixture density is closely related to both S_v and S_g as,

$$\rho_m = \rho + (\rho_s - \rho)S_v = \frac{\rho}{1 - S_g + \rho S_g/\rho_s} \quad (3\text{-}18)$$

Since $\rho << \rho_s$, the above equation can be simplified to,

$$\rho_m = \rho + \rho_s S_v = \frac{\rho}{1 - S_g} \quad (3\text{-}19)$$

The above equation also indicates there is a fixed relationship between S_v and S_g. Therefore, only one variable is necessary to represent the sediment concentration, and here

adopted volumetric concentration S_v, (hereafter, S, m^3/m^3). Then the mixture density gradient, or - $d\rho_m/dz$ (negative sign is to keep the gradient positive) can be expressed as,

$$-d\rho_m / dz = -\rho_s dS / dz \qquad (3\text{-}20)$$

3.5.6 Sedimentological Richardson number

The Richardson number can be expressed as a density-gradient Richardson number R_i or density-flux Richardson number R_f. Combining equations 2-26, 3-19 and 3-20, R_i can be expressed as,

$$R_i(z) = \frac{-\rho_s g /(\rho + S\rho_s) \cdot dS / dz}{(du / dz)^2} \qquad (3\text{-}21)$$

From equation 2-29, flux Richardson number requires direct measurement of w' at elevation z. However, if z is too low, the required sampling rate to measure w' would be much greater than 32 Hz (van Boxel, et al., 2004), exceeding the maximum sampling frequency of the ultrasonic anemometer. Therefore, it is not practical to measure the local w'. An alternative method was proposed by Monin and Yaglom (1971). They assumed the sediment density flux is proportional to the mixture gradient, or,

$$\overline{\rho_m' w'} = \upsilon_s \frac{d\rho_m}{dz} \qquad (3\text{-}22)$$

After substituting equation 2-29 with equations 3-4, 3-19, 3-20, and 3-22, R_f can be expressed with the concentration gradient dS/dz and "true" shear velocity, u_*',

$$R_f = \frac{-g\upsilon_S(\rho_s / \rho - 1)dS / dz}{(u_*')^2 (du / dz)} \qquad (3\text{-}23)$$

where v_S is turbulent sediment eddy diffusivity in the stratified sediment laden flow. Following Herrmann and Madsen (2007), according to the conservation of mass flux:

$$w_s S + \upsilon_S \frac{dS}{dz} = 0 \qquad (3\text{-}24)$$

Therefore,

$$R_f = \frac{g w_s S / (\rho_s / \rho - 1)}{(u_*^{'})^2 (du/dz)} \qquad (3\text{-}25)$$

where w_s is sediment settling velocity, which can be estimated from a comprehensive experiment (Chen and Fryrear, 2001),

$$w_s = -0.775352 + 4.52657\sqrt{d} \qquad (3\text{-}26)$$

3.6 Summary

Ultrasonic anemometer, cup anemometer and hose traps were deployed from 2 to 5 min to collect velocity fluctuation components, wind velocity profile and sediment flux profile, respectively, which can be used to calculate mean grain size, apparent von Kármán parameter, sediment transport rate, concentration profile, and Richardson numbers for further analysis.

4. EXPERIMENT RESULTS AND DATA ANALYSIS

4.1 Results

We used 17 data sets to examine the variability of the apparent von Kármán parameter: 15 with aeolian saltation and 2 under "clear air" conditions. The surface elevation change during each run was very small (< 1cm), considered negligible compared to the absolute location of each sensor.

4.1.1 Anemometer measurement

The wind velocity profiles were measured by cup anemometers for the 17 runs (Table 4-1). After log-linear curve fitting on cup anemometer data, following the methods in section 3.5.2, slope m, shear velocity from wind profile measurement u_*, apparent roughness length z_{0a} and regression coefficient R^2 can be calculated (Table 4-1). Other wind profile data sets were also obtained. However, if the R^2 of the velocity profile was less than 0.985, these data were not considered further because of the degree of statistical uncertainty associated with estimates of m and z_0. Wind profiles from the cup anemometers have R^2 of at least 0.986.

Following the methods described in section 3.5.2, estimates of u_*', and κ_a from the anemometer measurements were derived (Table 4-1). The shear velocity estimates in clear air (runs 16 and 17) were obtained from the Reynolds stresses (equation 3-4) and the velocity profiles (equation 3-2). The Reynolds stress method had the shear velocity estimates of 0.373 m/s and 0.379 m/s, while the wind profile analysis indicated values of 0.390 m/s and 0.365 m/s. The corresponding κ values are 0.382 and 0.415, which are close to 0.4. The agreement between the κ estimates indicates that the approaches, described in section 3.5.2, are appropriate for the derivation of κ_a. These two values of κ were averaged to obtain a κ value of 0.399 in the clear air condition. Therefore the correction factor Φ_m for sediment-laden studies can be calculated by $\Phi_m = \kappa/\kappa_a = 0.399/\kappa_a$, also shown in Table 4-2.

Table 4-1 Wind profiles data obtained from cup anemometers

Run	T (s)	$u(z)$ (m/s)				R^2	m	z_{0a} (mm)	u_* (m/s)
		0.25 m	0.5 m	0.75 m	1 m				
1	120	7.21	8.57	9.19	9.53	0.991	1.694	3.400	0.676
2	180	6.86	8.21	8.81	9.12	0.988	1.656	3.799	0.661
3	180	7.23	8.62	9.32	9.66	0.992	1.783	4.185	0.711
4	213	6.72	8.06	8.70	9.03	0.991	1.693	4.553	0.676
5	170	7.36	8.66	9.18	9.67	0.995	1.650	2.806	0.658
6	240	6.95	8.12	8.49	9.02	0.989	1.456	2.059	0.581
7	240	6.93	8.06	8.48	8.92	0.993	1.415	1.806	0.564
8	240	7.04	8.11	8.56	8.96	0.996	1.375	1.463	0.549
9	240	6.83	7.86	8.16	8.62	0.986	1.257	1.054	0.501
10	240	7.16	8.21	8.61	9.05	0.994	1.340	1.170	0.535
11	240	6.51	7.47	7.93	8.42	0.997	1.352	2.018	0.540
12	300	6.05	7.07	7.46	7.96	0.993	1.347	2.772	0.538
13	240	7.99	8.96	-	9.94	1.000	1.402	0.836	0.559
14	299	7.98	8.96	-	9.97	1.000	1.434	0.958	0.572
15	240	8.11	9.11	-	10.11	1.000	1.441	0.897	0.575
16	612	9.09	9.80	-	10.44	0.999	0.976	0.022	0.389
17	644	8.94	9.56	-	10.21	1.000	0.913	0.014	0.364
Max	644	9.09	9.80	9.32	10.44	1.000	1.783	4.553	0.711
Min	120	6.05	7.07	7.46	7.96	0.986	0.913	0.014	0.364
Mean	273	7.35	8.44	8.57	9.33	0.994	1.423	1.989	0.568

Table 4-2 Estimates of u_*', κ_a and Φ_m from ultrasonic anemometer measurements

Run	u_*' (m/s)	κ_a	Φ_m
1	0.542	0.320	1.247
2	0.490	0.296	1.350
3	0.471	0.264	1.509
4	0.533	0.315	1.269
5	0.489	0.296	1.347
6	0.498	0.342	1.167
7	0.499	0.353	1.131
8	0.470	0.341	1.168
9	0.451	0.359	1.112
10	0.509	0.380	1.051
11	0.483	0.357	1.118

Table 4-2 Continued

Run	u_*' (m/s)	κ_a	Φ_m
12	0.413	0.306	1.303
13	0.497	0.354	1.126
14	0.499	0.348	1.146
15	0.491	0.341	1.170
16	0.373	0.382	1.045
17	0.379	0.415	0.961
max	0.542	0.415	1.51
min	0.373	0.264	0.96
mean	0.476	0.339	1.19

From Table 4-2, u_*' ranges from 0.373 to 0.542 m/s, about -21% to 14% different from the mean with saltation, κ_a ranges from 0.264-0.380 which is 66% to 89% of κ. In most cases, Φ_m is greater than 1 and can reach as high as 1.509. These results indicate that the Law of the Wall requires correction in order to correctly obtain "true" shear velocity estimates from the velocity profile in sediment-laden boundary layers. The modified Law of the Wall can be expressed as,

$$u = \frac{u_*'}{\kappa_a} \ln\left(\frac{z}{z_0}\right) \tag{4-1}$$

or,

$$u = \frac{u_*'}{\kappa} \phi_m \ln\left(\frac{z}{z_0}\right) \tag{4-2}$$

4.1.2 Hose trap measurement

Hose traps provided sand samples for estimating grain size distributions, sediment transport rates, and mass flux profiles. Following the methods described in section 3.5.1 and 3.5.3, mean grain size d, total mass flux M_t, sediment flux for each trap M, and sediment transport rate Q were obtained for sediment-laden runs (c.f. Table 4-3 and Table 4-4). While

calculating Q, some error may occur if sand is moving at elevations above the trap stack. However, our hose trap stack was about 0.55 m tall, and observations in the field revealed only minor transport above that height. Hence this error is negligible.

Table 4-3 d, M_t, Q and S for all hose trap runs

Run	d (mm)	M_t (kg)	Q (kg/m/s)
1	0.298	0.378	3.15×10^{-2}
2	0.217	0.433	2.40×10^{-2}
3	0.223	0.566	3.15×10^{-2}
4	0.235	0.465	2.18×10^{-2}
5	0.304	0.444	2.61×10^{-2}
6	0.294	0.490	2.04×10^{-2}
7	0.279	0.433	1.80×10^{-2}
8	0.284	0.373	1.56×10^{-2}
9	0.297	0.360	1.50×10^{-2}
10	0.298	0.433	1.81×10^{-2}
11	0.247	0.632	2.63×10^{-2}
12	0.270	0.609	2.03×10^{-2}
13	0.335	0.544	2.27×10^{-2}
14	0.432	0.489	1.64×10^{-2}
15	0.437	0.656	2.73×10^{-2}
Max	0.437	0.656	3.15×10^{-2}
Min	0.217	0.360	1.50×10^{-2}
Mean	0.297	0.487	2.23×10^{-2}

From Table 4-3, d varies from 0.217 mm to 0.437 mm, about –27% to 47% of the mean value of 0.297 mm, M_t varies by about -26% to 34% of the mean of 0.487 kg, and Q has a variation of -32% to 41% around the mean of 2.23×10^{-2} kg/m/s.

Table 4-4 Sediment mass flux M (in kg) collected in each trap for each sediment-laden run

Run	Trap 1	Trap 2	Trap 3	Trap 4	Trap 5	Trap 6	Trap 7	Trap 8	Total
1	0.1051	0.0739	0.0641	0.0364	0.0316	0.0387	0.0157	0.0124	0.3779
2	0.1299	0.0919	0.0854	0.0305	0.034	0.0302	0.0163	0.0145	0.4327

Table 4-4 Continued

Run	Trap 1	Trap 2	Trap 3	Trap 4	Trap 5	Trap 6	Trap 7	Trap 8	Total
3	0.2065	0.1210	0.0925	0.0456	0.0402	0.0321	0.0147	0.0135	0.5661
4	0.139	0.0781	0.1127	0.0547	0.0409	0.0222	0.0097	0.0076	0.4649
5	0.1488	0.0765	0.0891	0.0451	0.0178	0.0167	0.0208	0.0291	0.4439
6	0.1658	0.0916	0.1041	0.0520	0.0301	0.0273	0.0102	0.0092	0.4903
7	0.1587	0.0902	0.0369	0.0928	0.0194	0.0169	0.0089	0.0089	0.4327
8	0.1298	0.0722	0.0754	0.0474	0.0247	0.0073	0.0077	0.0087	0.3732
9	0.1248	0.0685	0.0727	0.0360	0.0228	0.0182	0.0089	0.0084	0.3603
10	0.1673	0.0771	0.0933	0.0331	0.0251	0.0196	0.0095	0.0083	0.4333
11	0.1727	0.1225	0.1362	0.076	0.0458	0.0413	0.0242	0.0128	0.6315
12	0.1600	0.1364	0.1531	0.0779	0.0355	0.0278	0.0109	0.0078	0.6094
13	0.2006	0.1221	0.1228	0.0523	0.0243	0.0145	0.0049	0.0029	0.5444
14	0.1149	0.0778	0.1056	0.0688	0.0443	0.0471	0.0207	0.0097	0.4889
15	0.1442	0.1057	0.1432	0.0898	0.0655	0.0654	0.0286	0.0131	0.6555

Following the method described in section 3.5.3, continuous sediment flux profiles can be predicted from exponential curve fitting between the geometric center z_{gc} (Table 4-5) and the normalized mass flux q (Table 4-6) for each trap. The results of the curve fitting including coefficients α and β and R^2 are listed in Table 4-7.

The exponential law describes the mass flux profiles well with $R^2 > 0.98$ except for Run 7 ($R^2 = 0.97$). There is a relative large distribution for α, about - 48% to 76% difference from the mean. There is a smaller range for β, from -7.599 to -12.419, or -28% to 38% of the mean. The root mean squared error (RMSE) is also calculated for each run with mean of 0.010 kg/m^2/s.

Table 4-5 Trap vertical opening and geometric center (z_{gc}) used for each run

	Trap 1	Trap 2	Trap 3	Trap 4	Trap 5	Trap 6	Trap 7	Trap 8
Trap vertical opening (m)	0.25	0.25	0.50	0.50	0.50	0.10	0.10	0.10
z_{gc} (m)	*	0.458	0.917	0.153	0.214	0.296	0.407	0.518

Note:*, z_{gc} for bottom trap =sqrt (0.25 z_{0a}).

Table 4-6 Normalized mass flux q for each run (kg/m^2/s)

Run	Trap 1	Trap 2	Trap 3	Trap 4	Trap 5	Trap 6	Trap 7	Trap 8
1	0.3503	0.2463	0.1068	0.0607	0.0527	0.0323	0.0131	0.0103
2	0.2887	0.2042	0.0949	0.0339	0.0378	0.0168	0.0091	0.0081
3	0.4589	0.2689	0.1028	0.0507	0.0447	0.0178	0.0082	0.0075
4	0.2610	0.1467	0.1058	0.0514	0.0384	0.0104	0.0046	0.0036
5	0.3501	0.1800	0.1048	0.0531	0.0209	0.0098	0.0122	0.0171
6	0.2763	0.1527	0.0868	0.0433	0.0251	0.0114	0.0043	0.0038
7	0.2645	0.1503	0.0308	0.0773	0.0162	0.0070	0.0037	0.0037
8	0.2163	0.1203	0.0628	0.0395	0.0206	0.0030	0.0032	0.0036
9	0.2080	0.1142	0.0606	0.0300	0.0190	0.0076	0.0037	0.0035
10	0.2788	0.1285	0.0778	0.0276	0.0209	0.0082	0.0040	0.0035
11	0.2878	0.2042	0.1135	0.0633	0.0382	0.0172	0.0101	0.0053
12	0.2133	0.1819	0.1021	0.0519	0.0237	0.0093	0.0036	0.0026
13	0.3343	0.2035	0.1023	0.0436	0.0203	0.0060	0.0020	0.0012
14	0.1537	0.1041	0.0706	0.0460	0.0296	0.0158	0.0069	0.0032
15	0.2403	0.1762	0.1193	0.0748	0.0546	0.0273	0.0119	0.0055

Table 4-7 Results of fitting exponential curve to the normalized mass flux profiles

Run	α	β	R^2	RMSE (kg/m2/s)
1	0.392	-11.646	0.981	0.019
2	0.332	-12.435	0.986	0.013
3	0.541	-15.991	0.991	0.016
4	0.283	-11.317	0.986	0.012
5	0.388	-14.677	0.990	0.013
6	0.299	-13.380	0.996	0.006
7	0.290	-15.199	0.932	0.026
8	0.231	-13.262	0.994	0.006
9	0.221	-13.627	0.997	0.004
10	0.299	-15.991	0.992	0.009
11	0.312	-10.219	0.997	0.006
12	0.245	-9.460	0.983	0.012
13	0.358	-13.262	0.999	0.004
14	0.157	-8.224	0.998	0.003
15	0.248	-7.599	0.999	0.003
max	0.541	-7.599	0.999	0.026

Table 4-7 Continued

Run	α	β	R^2	RMSE (kg/m2/s)
min	0.157	-15.991	0.932	0.003
mean	0.306	-12.419	0.988	0.010

The predicted flux profiles are plotted in Figure 4-1. Sediment flux decreases exponentially with elevation. Among these profiles, Run 3 has steepest slope and Run 14 has the flattest. The cumulative distribution profiles of q are plotted in Figure 4-2. From the figures, when z is at about 0.1 m, the slope of q profiles and cumulative distribution profiles decreases dramatically, indicating this elevation may be considered as the upper limit of the saltation layer (about 50% to 80% total transport occurs below z = 0.1 m).

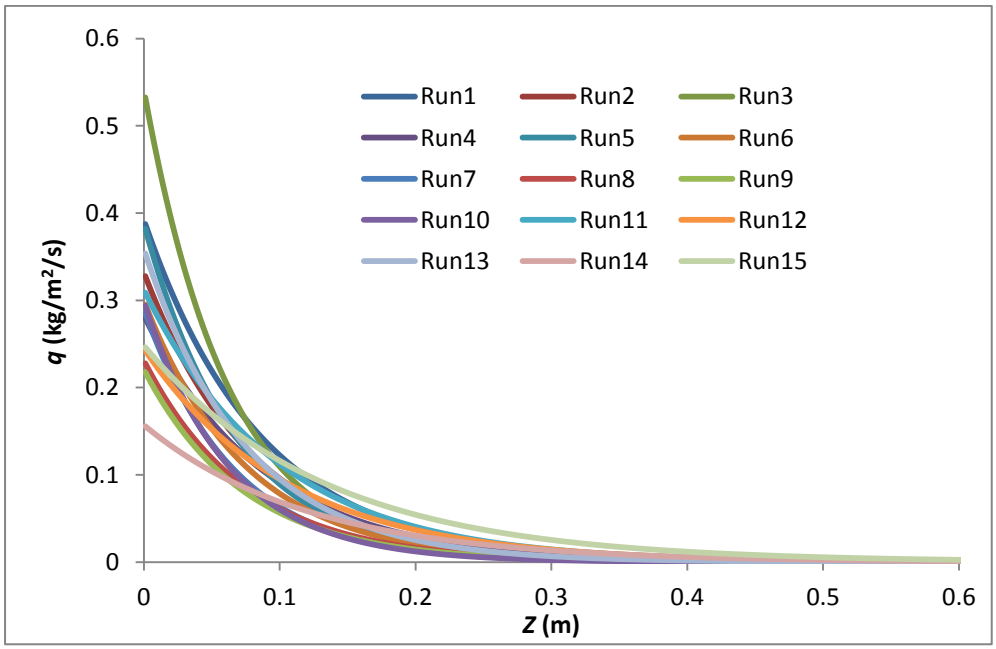

Figure 4-1 Predicted normalized flux profiles.

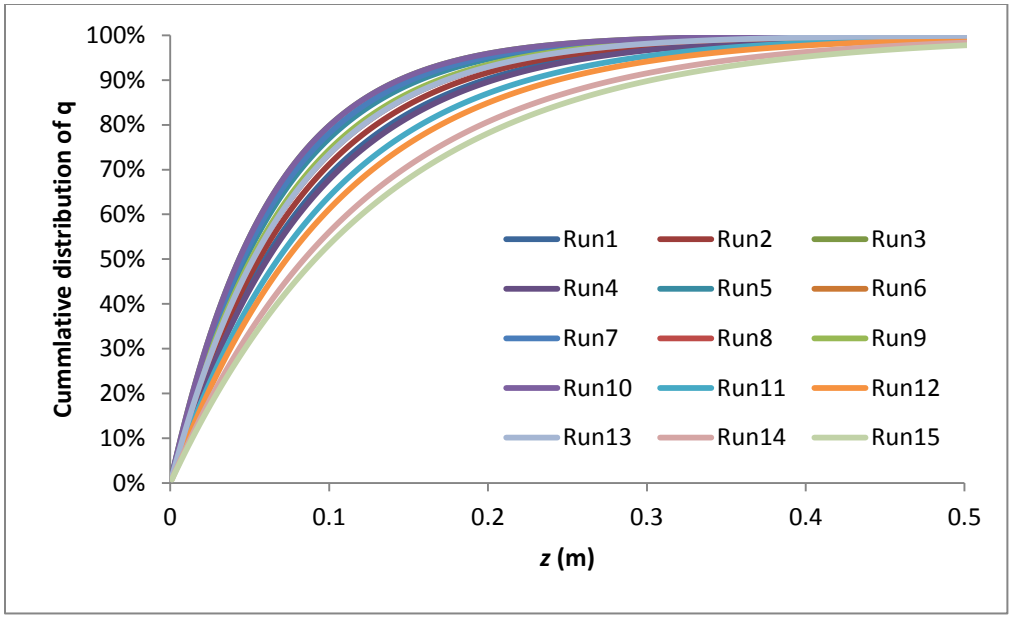

Figure 4-2 Cumulative distribution of q (%) using the predicted profiles.

4.2 Data analysis

4.2.1 Velocity profile correction

As discussed in section 3.5.4, the velocity profile may not be log-linear when entering the saltation layer. Two methods (Owen, 1980; Li et al., 2004) were used to estimate the saltation layer thickness, H_s, to correct the velocity profile inside the saltation layer. In Figure 4-3, two corrected profiles and one uncorrected profile for Run 1 are plotted. Apparently, velocity will be significantly underestimated and roughness length will be greatly overestimated if the "log" profile line is extrapolated into the saltation layer. The modified roughness length z_{0s} and saltation layer thickness H_s (Subscript 1for Owen, 1980 and 2 for Li et al., 2004) for each sediment-laden run is listed in Table 4-8. The averaged saltation height from Owen's method is about 0.02 m, which is smaller than the average value of 0.085 m from Li. et al. (2004). The latter appears more reasonable since it represents the flux weighted average saltation height and

it is quite close to the elevation where the slope of the flux decreases dramatically (c.f. Figure 4-2). Therefore, in this study, the velocity profile modeled from Li et al. (2004) was adopted.

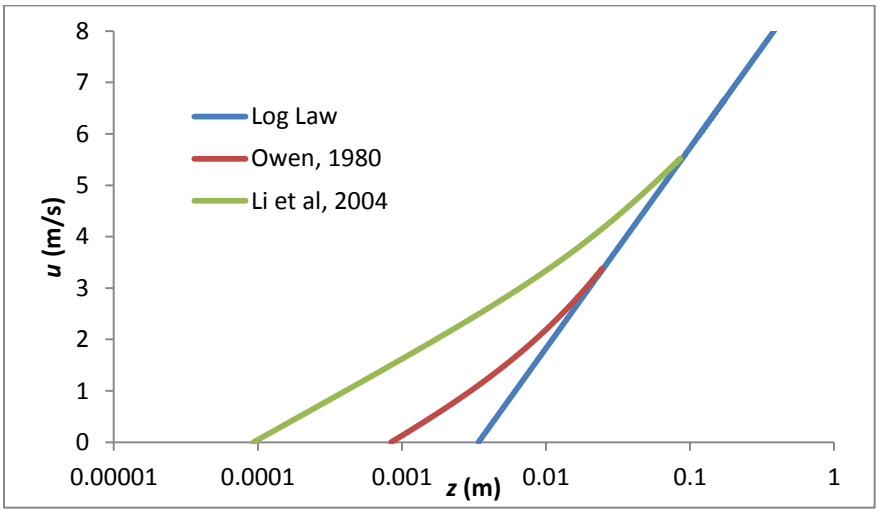

Figure 4-3 Corrected and uncorrected velocity profiles near bed for Run 1.

Table 4-8 Saltation layer thickness H_s (m) and Corrected roughness length z_{0s} (m). Subscript 1 refers to the data from Owen (1980) and subscript 2 refers to data from Li et al. (2004). For comparison, uncorrected apparent roughness length z_{0a} (m) is also listed.

Run	H_{s1}	H_{s2}	z_{0s1}	z_{0s2}	z_{0a}
1	0.025	0.086	8.36E-04	1.00E-04	3.40E-03
2	0.020	0.080	1.33E-03	1.10E-04	3.80E-03
3	0.019	0.063	1.83E-03	2.63E-04	4.19E-03
4	0.024	0.088	1.53E-03	1.21E-04	4.55E-03
5	0.020	0.068	8.47E-04	1.54E-04	2.81E-03
6	0.021	0.075	3.88E-04	5.62E-05	2.06E-03
7	0.021	0.066	2.60E-04	4.15E-05	1.81E-03
8	0.018	0.075	2.37E-04	3.30E-05	1.46E-03
9	0.017	0.073	1.57E-04	2.55E-05	1.05E-03
10	0.022	0.063	9.10E-05	1.72E-05	1.17E-03
11	0.019	0.098	3.67E-04	2.57E-05	2.02E-03
12	0.014	0.106	1.40E-03	1.61E-04	2.77E-03
13	0.021	0.075	6.60E-05	1.15E-05	8.36E-04
14	0.021	0.122	1.45E-04	2.33E-05	9.58E-04
15	0.020	0.132	1.43E-04	2.24E-05	8.97E-04

Table 4-8 Continued

Run	H_{s1}	H_{s2}	z_{0s1}	z_{0s2}	z_{0a}
Max	0.025	0.132	1.83E-03	2.63E-04	4.55E-03
Min	0.014	0.063	6.60E-05	1.15E-05	8.36E-04
Mean	0.020	0.085	6.42E-04	7.77E-05	2.25E-03

The uncorrected apparent rough length z_{0a} is one order of magnitude higher than z_{0s2} and two orders of magnitude higher than z_{0s1}. The former is the function of shear velocity (Sherman 1992), which controls saltation conditions, and the latter two are more close to the concept of grain roughness, which is controlled by grain size (Nikuradse, 1932). Here after, z_{0s} and H_s refer to the corresponding values derived from Li et al. (2004).

4.2.2 Volumetric concentration profiles

With normalized flux profile and velocity profile, volumetric concentration for each trap has been calculated according to equation 3-16 (Table 4-9). From the table, *S* decreases dramatically from Trap 1 (bottom) to Trap 8 (top). Continuous volumetric concentration profiles calculated from velocity profiles and mass flux profiles confirm this trend (Figure 4-3).

Table 4-9 Volumetric concentration *S* for each run (m^3/m^3).

Run	Trap 1	Trap 2	Trap 3	Trap 4	Trap 5	Trap 6	Trap 7	Trap 8
1	4.03E-05	1.94E-05	7.25E-06	3.57E-06	2.86E-06	1.62E-06	6.12E-07	4.39E-07
2	3.61E-05	1.72E-05	6.83E-06	2.10E-06	2.16E-06	8.83E-07	4.43E-07	3.58E-07
3	6.15E-05	2.26E-05	7.12E-06	3.00E-06	2.43E-06	8.92E-07	3.79E-07	3.16E-07
4	3.41E-05	1.28E-05	7.87E-06	3.28E-06	2.25E-06	5.60E-07	2.27E-07	1.61E-07
5	4.08E-05	1.40E-05	6.93E-06	3.05E-06	1.12E-06	4.85E-07	5.65E-07	7.19E-07
6	3.07E-05	1.20E-05	5.96E-06	2.62E-06	1.41E-06	5.96E-07	2.09E-07	1.72E-07
7	2.92E-05	1.19E-05	2.10E-06	4.67E-06	9.12E-07	3.70E-07	1.83E-07	1.67E-07
8	2.23E-05	9.08E-06	4.19E-06	2.34E-06	1.14E-06	1.58E-07	1.57E-07	1.62E-07
9	2.13E-05	8.71E-06	4.10E-06	1.82E-06	1.08E-06	4.06E-07	1.88E-07	1.62E-07
10	2.78E-05	9.55E-06	5.06E-06	1.60E-06	1.14E-06	4.17E-07	1.91E-07	1.53E-07
11	3.20E-05	1.68E-05	8.28E-06	4.11E-06	2.31E-06	9.69E-07	5.33E-07	2.57E-07
12	2.85E-05	1.66E-05	8.12E-06	3.65E-06	1.54E-06	5.59E-07	2.05E-07	1.33E-07

Table 4-9 Continued

Run	Trap 1	Trap 2	Trap 3	Trap 4	Trap 5	Trap 6	Trap 7	Trap 8
13	2.81E-05	1.31E-05	5.90E-06	2.26E-06	9.91E-07	2.78E-07	8.91E-08	4.84E-08
14	1.26E-05	6.55E-06	4.02E-06	2.40E-06	1.45E-06	7.26E-07	3.02E-07	1.30E-07
15	1.92E-05	1.08E-05	6.62E-06	3.83E-06	2.63E-06	1.24E-06	5.12E-07	2.15E-07

Three distinct layers can be identified from these profiles: 1) Surface roughness layer. The upper limit of this layer is from one-hundredth to one-tenth of the grain size, well within a grain diameter. The velocity of this layer is close to zero, *S* decreases from 10^0 (m^3/m^3) at z_{0s} to the order of 10^{-4} at the top of the roughness layer. 2) Saltation layer. Above the roughness layer to H_s, where most saltating grains are concentrated, *S* only drops less than 2 orders of magnitude to 10^{-6}. 3) Constant shear stress layer. Above the saltation layer, grains with higher energy may reach here, where *S* decreases faster than it does within the saltation layer. In this layer, wind speed profile remains log-linear, the Reynolds stress remains constant.

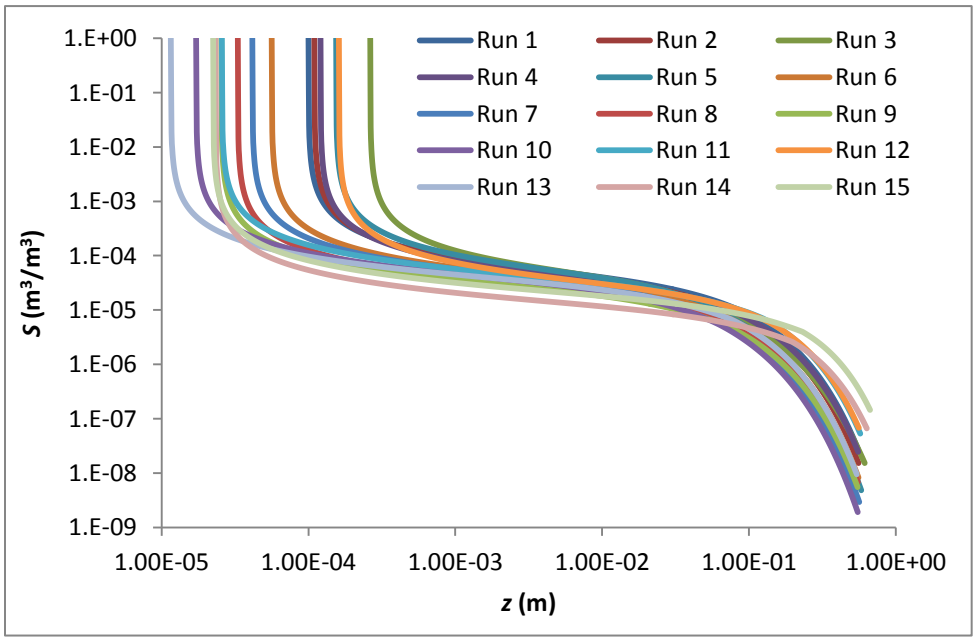

Figure 4-3 Volumetric concentration profiles.

4.2.3 Density gradient

From equation 3-19, the density gradient, - $d\rho_m/dz$ is proportional to - dS/dz. Therefore, using the profile of S, the density gradient profile can be obtained (Figure 4-4).

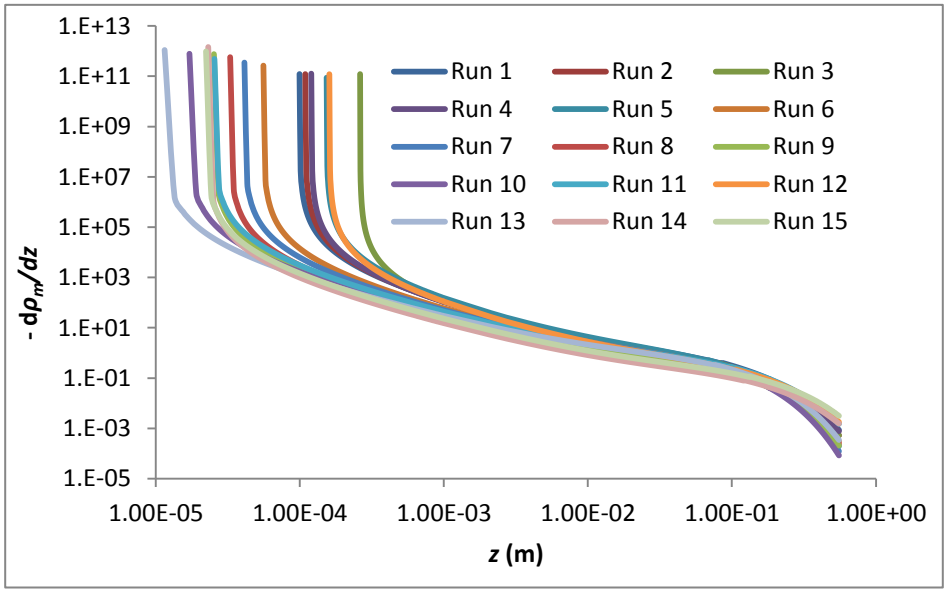

Figure 4-4 Mixture density gradient profile for all runs.

The same three layers (surface roughness layer, saltation layer and constant shear stress layer), can be easily identified through inspecting the slope of the profiles. The limits separating these layers are identical to those found in the S profiles.

4.2.4 Sedimentological Richardson numbers

Both the sedimentological gradient Richardson number R_i and the sedimentological flux Richardson number R_f have been calculated using the method in section 3.5.6. For R_i profiles (Figure 4-5), R_i decreases dramatically (3 to 5 orders of magnitude) in the roughness layer, but increases (1 to 2 orders of magnitude) in the saltation layer, and then decreases again in the constant shear stress layer. Note there is a “step” at the top of saltation layer, which is caused by

the discontinuity of the velocity gradient, *du/dz*, caused by merging the semi-log profile with the Li et al. (2004) profile. A similar pattern is also found in the profiles of R_f (Figure 4-6). Both R_i and R_f are greater than 0, indicating the turbulence vertical mixing should be damped.

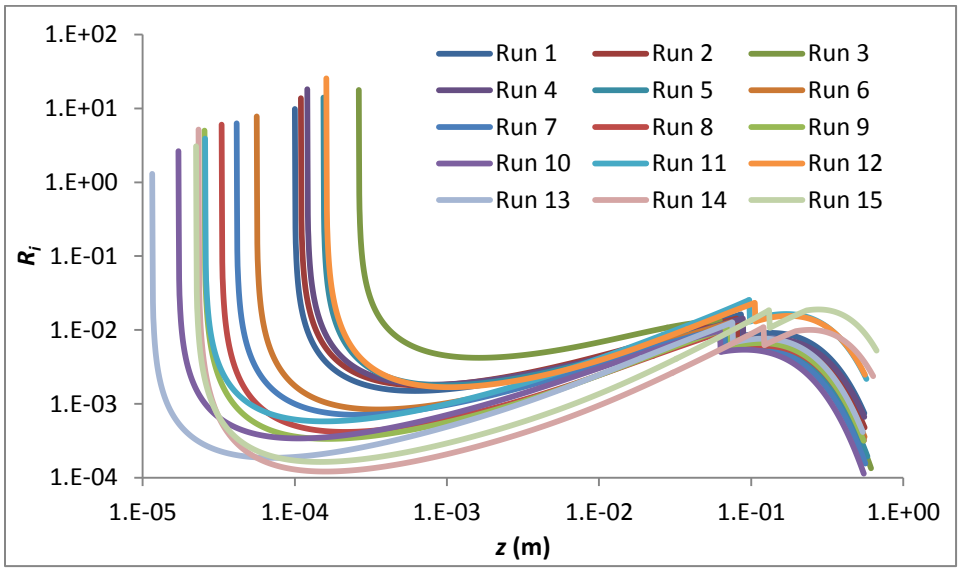

Figure 4-5 Sedimentological gradient Richardson number profiles.

To evaluate the average effect of stratification effects within the saltation layer, the average Richardson numbers (R_{ia} and R_{fa}) between apparent roughness length z_{0a} to saltation height H_s can be calculated by:

$$R_{ia} = \frac{1}{H_s - z_{0a}} \int_{z_{0a}}^{H_s} R_i dz \qquad (4\text{-}3)$$

and

$$R_{fa} = \frac{1}{H_s - z_{0a}} \int_{z_{0a}}^{H_s} R_f dz \qquad (4\text{-}4)$$

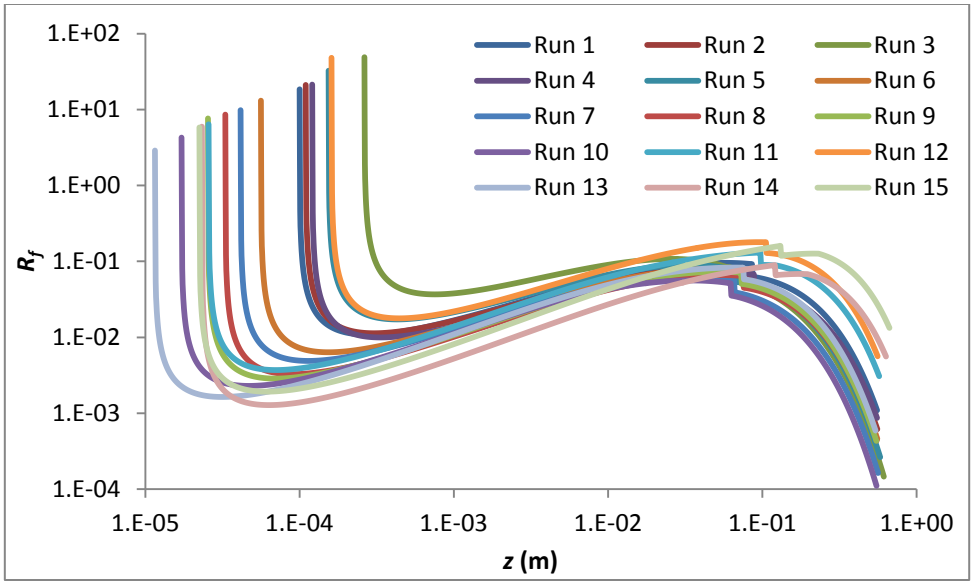

Figure 4-6 Sedimentological flux Richardson number profiles.

The results of R_{ia} and R_{fa} for each run are displayed in Table 4-10. R_{fa} has a range from 0.036 to 0.110 and R_{ia} from 0.002 to 0.009, which are close to the values found in some sediment-laden water studies (e.g. Adams and Weatherly, 1981; Wright and Parker, 2004). Positive Richardson numbers also imply that the flow in the saltation layer is stably stratified.

Table 4-10 Average Richardson numbers R_{fa} and R_{ia} for each run

Run	R_{fa}	R_{ia}
1	0.071	0.007
2	0.063	0.007
3	0.093	0.009
4	0.056	0.007
5	0.070	0.005
6	0.055	0.005
7	0.046	0.004
8	0.042	0.004
9	0.044	0.003
10	0.038	0.004
11	0.076	0.008

Table 4-10 Continued

Run	R_{fa}	R_{ia}
12	0.110	0.008
13	0.046	0.003
14	0.036	0.002
15	0.060	0.004
max	0.110	0.009
min	0.036	0.002
mean	0.060	0.005

4.3 Hypotheses test

4.3.1 Relationship between *d* and κ_a

To test hypothesis 1, regression analysis has been conducted between mean grain size *d* and κ_a (Figure 4-7). The result shows that there is not a significant linear relationship at 95% confidence level ($p = 0.117$), which may be due to the small grain size range found at the study site or small sample size. The relationship between d and κ_a cannot be confirmed.

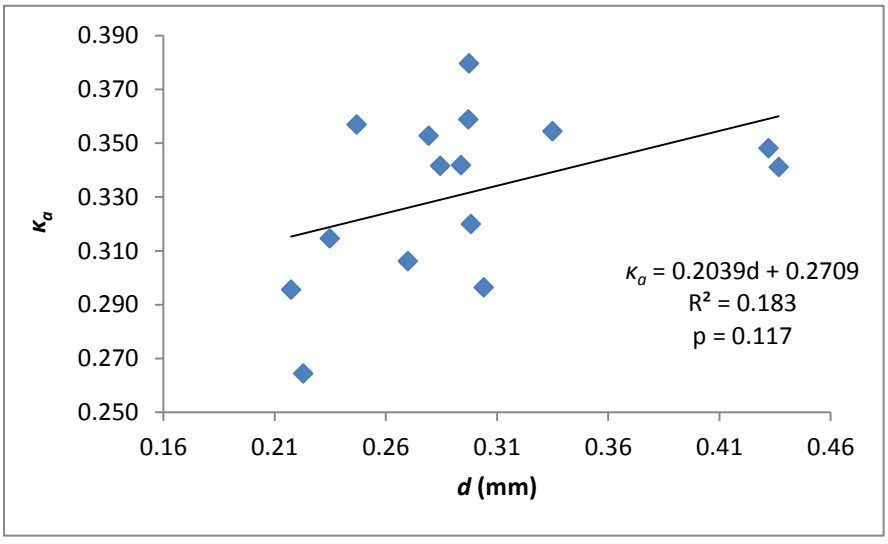

Figure 4-7 Results of regression analysis between *d* and κ_a.

4.3.2 Relationship between S and κ_a

To test hypothesis 2, linear regression analysis has been performed using estimates of κ_a and the S profile between 0.001 and 0.5 m (κ_a is the dependent variable). R^2 and p values from the regression analysis are plotted in Figure 4-8.

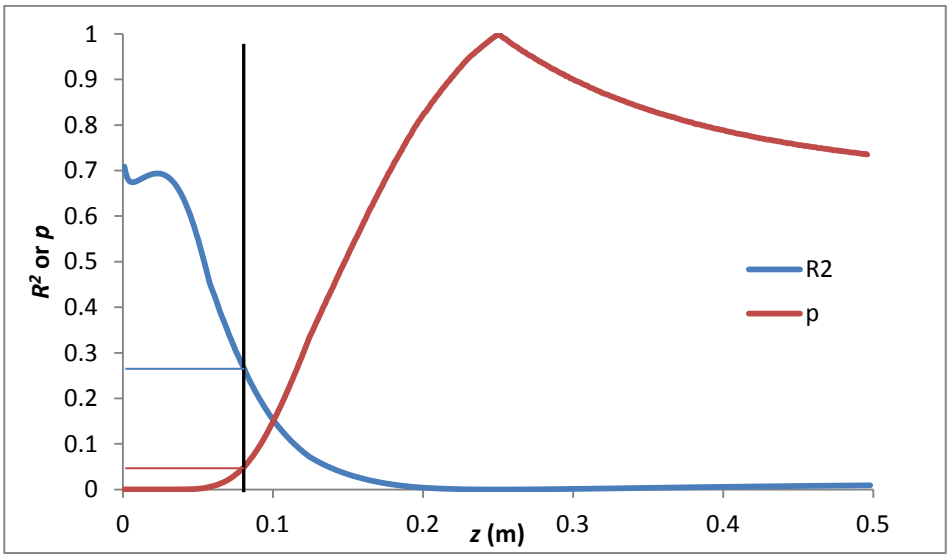

Figure 4-8 R^2 and p values for regression analysis between κ_a and S_v profile, when z = 0.081 m, p = 0.005 and R^2=0.264.

The regression analysis shows that R^2 decreases and p increases with the increase of elevation. When z >0.081 m, p >0.05, indicating the relationship between κ_a and S_v is not statically significant at 95% confidence level. The cutoff of 0.081 m matches well with the mean saltation layer height of 0.085 m. This indicates that the eddy size may be related to the sand concentration within saltation layer and when z > 0.081m, S is too small to influence the scale of eddies. R^2 has the highest value near the bed. Therefore, it is reasonable to use the S_{25} values derived from the bottom trap (i.e. Trap 1) to predict the trend of κ_a (subscript 25 indicates S value

of 0 < z < 25 mm, which covers the opening range of Trap 1). Regression analysis has confirmed the significance of their relationship with $R^2 = 0.70$ and $p < 0.001$ (Figure 4-9).

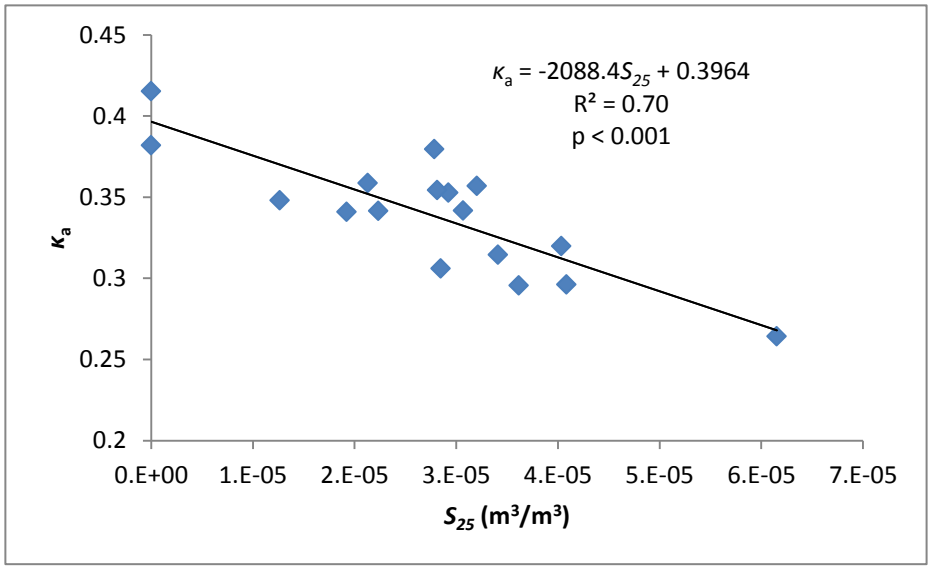

Figure 4-9 Results of linear regression between S_{25} and κ_a. This analysis also includes the runs in clear air flow with $S_{25} = 0$ (Runs 16 and 17).

4.3.3 Relationship between sedimentological Richardson numbers and κ_a

Regression analysis was performed to test hypothesis 3. R^2 and p for R_i and κ_a are displayed in Figure 4-10, and for R_f and κ_a, in Figure 4-11.Unlike the relationship between S and κ_a, the cutoff of p =0.05 for κ_a and R_i regression is at z = 0.042 m and for κ_a and R_f regression is at 0.034 m. This means that within this range, κ_a is proportional to R_i or R_f at the 95% confidence level. Therefore, the variability of κ_a is not statistically significant relative to the stratification conditions where z > 0.05 m or $S < 10^{-5}(m^3/m^3)$. Since either R_i or R_f is a function of z, the elevation selection becomes critical in evaluating the relationships. In order to avoid the arbitrary selection of elevation, concentration weighted average Richardson numbers, R_{ia} and R_{fa}, were

employed here to present the bulk stratification effect from the saltation layer, where the highest density gradient is found.

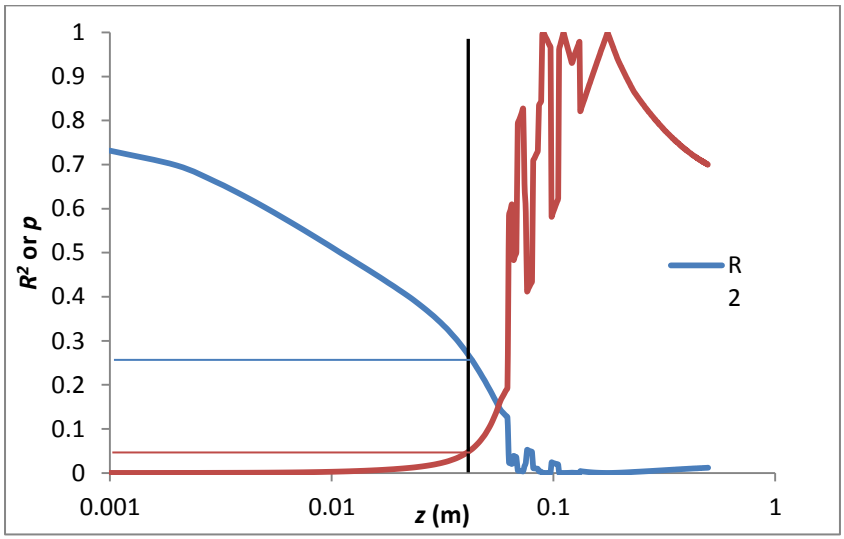

Figure 4-10 R^2 and p values for regression analysis between κ_a and R_i profile, when z = 0.042 m, p = 0.05 and R^2 = 0.264. The fluctuation of the curves near z = 0.1 m is due to the discontinuities of du/dz at saltation layer top for the first 15 runs.

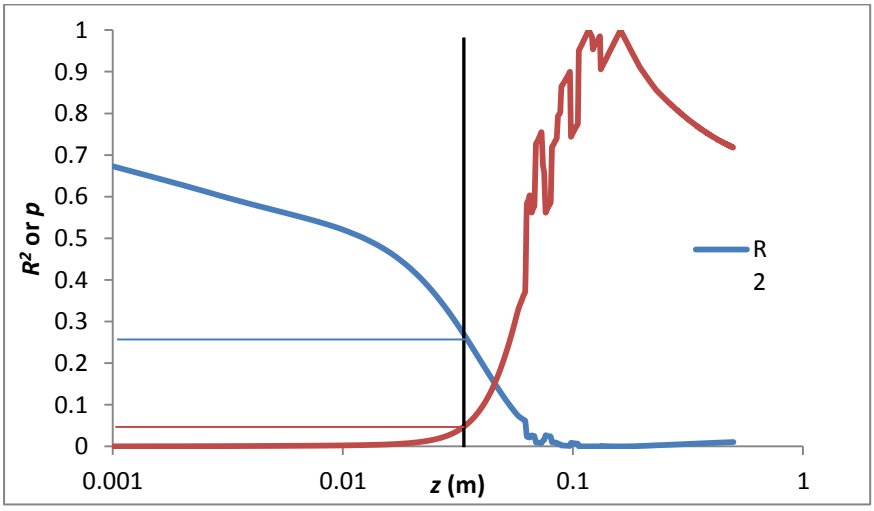

Figure 4-11 R^2 and p values for regression analysis between κ_a and R_f profile, when z = 0.034 m, p = 0.05 and R^2=0.264. The fluctuation of the curves near z = 0.1 m is due to the discontinuities of *du/dz* at saltation layer top for 15 runs.

Regression analysis between κ_a and R_{ia}, and between κ_a and R_{fa} shows their relationships are statistically significant at 99.9% confidence level. The results are depicted in Figure 4-12 and Figure 4-13. According to equation 2-31, there is a linear relationship between κ_a/κ and either Richardson number as:

$$\frac{1}{\Phi_m} = \frac{\kappa_a}{\kappa} = 1 - \lambda R_f = 1 - Sc\lambda R_i \qquad (4\text{-}5)$$

In order to obtain Schmidt number Sc and damping coefficient λ, the regression functions were adjusted with the intercept = 1, and,

$$\kappa_a / \kappa = 1 - 31.270 R_{ia} \quad \text{with } R^2 = 0.66 \qquad (4\text{-}6)$$

$$\kappa_a / \kappa = 1 - 2.7877 R_{fa} \text{ with } R^2 = 0.67 \qquad (4\text{-}7)$$

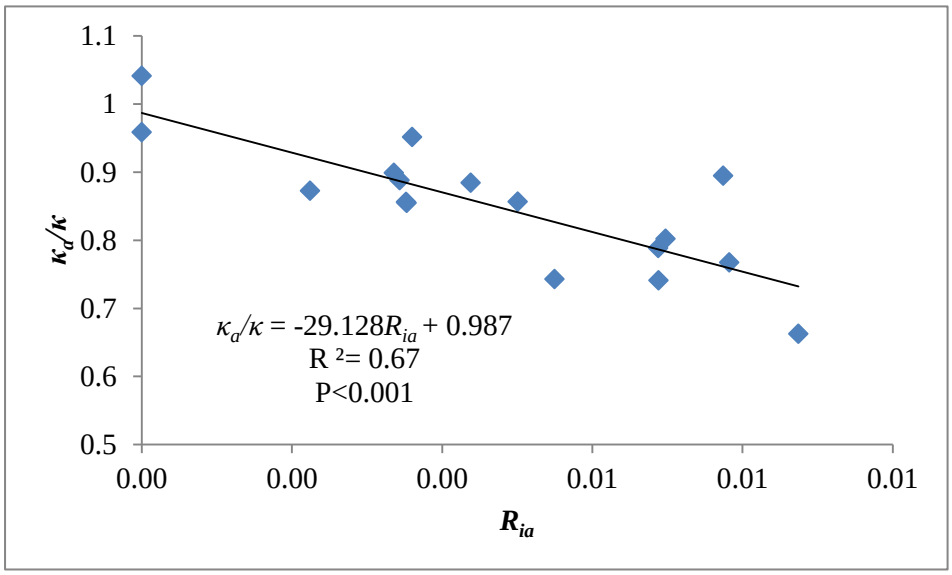

Figure 4-12 Results of linear regression between R_{ia} and κ_a. This analysis includes the runs in clear air flow with R_{ia} = 0 (Runs 16 and 17).

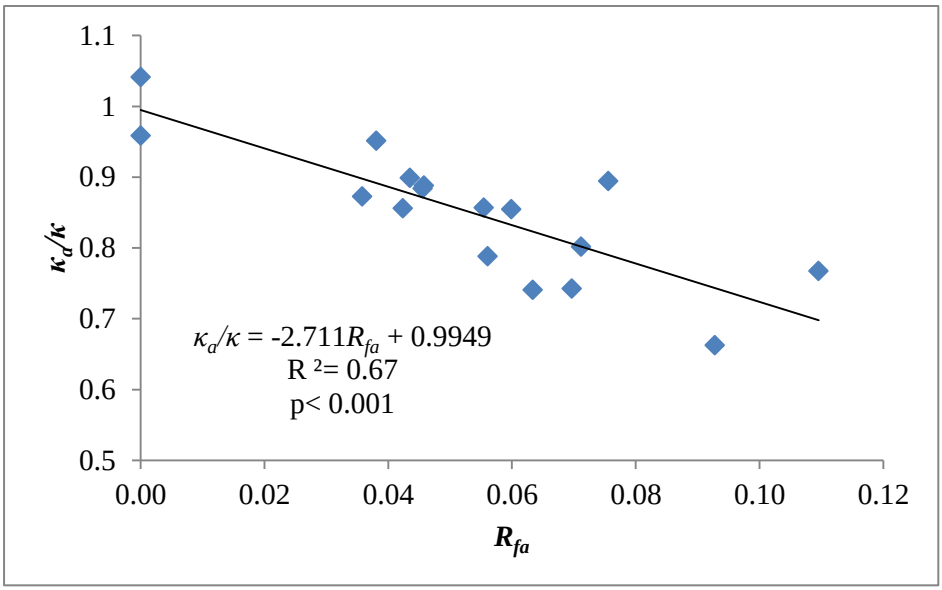

Figure 4-13 Results of linear regression between R_{fa} and κ_a. This analysis includes the runs in clear air flow with R_{fa} = 0 (Runs 16 and 17).

The coefficients of determination from equations 4-6 and 4-7 are only slightly smaller than those shown in the Figure 4-12 and Figure 4-13. From equation 4-5 to 4-7, it is easy to conclude that λ = 2.79 and Sc = 11.22. The Schmidt number is > 1, indicating that the sediment diffusivity is greater than eddy viscosity during aeolian saltation, which is similar to the results of some sediment stratified water experiments (e.g., 1 to 10 by Lees, 1981); the damping coefficient is a smaller than the typical values of 6.9 to 10 in sediment stratified water flow (c.f. section 2.4) but larger than the values in the thermally stratified air flow (1.05 or 1.35, c.f. section 2.2). This implies that the characteristics of sediment-laden air flow are similar to that of sediment-laden water flow.

4.4 Summary

In this section, the experimental and analytical results have been described. Regression analysis indicates that there is a significant linear relationship between the apparent von Kármán

parameter and sediment concentration within the saltation layer. A linear relationship is also significant between apparent von Kármán parameter and Richardson numbers at lower elevations within the saltation layer. However, the relationship between apparent von Kármán parameter and sand grain size is not statistically significant.

5. DISCUSSION

Analysis of experiment results shows the statistically significant relationships between the von Kármán parameter κ_a and sediment concentration S and Richardson numbers, and the not significant relationship with sediment grain size d. In this section, I will discuss theories that may explain these relationships, the experimental errors, the implications and limitations of this study.

5.1 Theoretical explanations

5.1.1 Supporting energy theory vs. stratification theory

The supporting energy theory implies that κ_a is a function of d and S. However, linear regression between κ_a and d does not yield a statistically significant relationship. On the other hand, the weighted, average sedimentological Richardson numbers, representing the stratification effect, do produce a satisfactory significant explanation of the variability in κ_a. This suggests that the stratification theory is more appropriate to explain the decrease of κ_a during aeolian saltation, especially because a profound density gradient exists in the saltation layer.

5.1.2 Thermal stratification vs. sedimentological stratification

As discussed in section 2.2, thermal stratification may also lead to the variation of κ_a. However, I expect the thermal stratification effect to be negligible compared to stratification effects caused by the presence of a saltation layer. For site B, the sand surface was wet, and air temperature was close to the surface temperature. Therefore there should not be a significant temperature gradient near the surface. For site A, the sand surface temperature was higher than the air temperature during some runs. However, the temperature gradient (order of 10^1 K/m), compared to the mixture density gradient (order of 10^{14} kg/m^4), should be small. Even if it is assumed that there is a considerable temperature gradient, with cold air overlaying warm air, the unstable air mixing would stretch the eddy size. This would lead to κ_a increase rather than

decrease, as shown in the experimental results. Therefore, the variation of κ_a was controlled by the sedimentological stratification effect.

5.2 Error analysis

For any experiment, errors (differences between expected results and measured results) always occur due to imperfect experimental design, instrument accuracy, statistical uncertainty and insufficient knowledge of the internal physics. The major sources of potential errors have been listed to evaluate the accuracy of this experiment.

5.2.1 Errors in velocity profile estimation

Wind velocity profiles were measured with cup anemometers. There are three main sources of potential errors in estimating profile slope *m* with the instruments:

1) Curve fitting. Errors may occur when estimating *m* and z_0 from the log normal curve fitting. To assess the magnitude of such errors, the standard errors of the *m* of the 15 hose trap runs were calculated. These averaged 5%, with a maximum of 9% for the lowest R^2 value of 0.985.

2) Cup anemometer calibration. The cup anemometers were calibrated using the manufacture's specifications, with approximately 2% to 3% error in wind speed. This may cause about up to about 5% error in *m* estimation.

3) Bed elevation change. Field observation indicates that there was less than 10 mm bed elevation rise/fall during each run, which could cause a maximum of 3 % error in *m* estimation.

Any errors in *m* will be transferred to κ_a and *S*, and this will cause 3 fold errors on R_{ia} and 2 fold errors in R_{fa} according to equations 3-21 and 3-25. For example, 5% error in m would lead to 16% error in R_{ia} and 10% error in R_{fa}.

Inside the saltation layer, the wind velocity was not measured directly because of the bulky size of cup anemometer. Instead, it is estimated using the physical model proposed by Li et al. (2004), which is a function of the sediment mass flux profile and threshold shear velocity.

This model has been verified by several wind tunnel experiments (Li et al., 2004), and the mass flux profile and threshold shear velocity used here were estimated from observed data. Therefore, I expect that the velocity profile estimates would not have too large errors. However, the accuracy of the profiles in the saltation layer is difficult to determine for these experiments because no data were obtained within that layer.

5.2.2 Errors in Reynolds stress measurement

Van Boxel et al. (2004) argued that the accuracy of Reynolds stress measurement depends on the ultrasonic anemometer deployment height, sampling rate and duration. As the elevation of the anemometer increases, to keep the same level of Reynolds stress accuracy, the required sampling duration becomes longer and the required sampling rate becomes slower. For all 17 runs, the ultrasonic anemometer was deployed at about 1 m above the bed, the sampling rate was set at 32 Hz and the sampling duration was least 2 minutes. Under these conditions, the error in u_*' estimation should be less than 5%.

5.2.3 Errors in sediment flux estimation

Substantial spanwise variability in sand transport rates has been found in studies of aeolian sediment transport systems, averaging 20-25% over a distance of 1 m and duration of 10-15 min (Gares et al., 1996; Jackson et al., 2006). The hose-trap array, cup anemometer array and the ultrasonic anemometer have a spanwise distance less than 2 m, which is large enough to have errors of 25% or larger in sediment transport rate or sediment concentrations.

The sediment transport rate, Q, was calculated from total mass flux caught in the traps. The sediment flux above 0.555 m was neglected because no trap was deployed above that level. After extrapolating the flux profile, the total mass flux above 0.555 m is only 0.7% to 6.6% of that below 0.555 m, with the average of 2.23%. However, this error is much smaller than the likely spanwise variability.

To evaluate the accuracy of mass-flux profile curve-fitting, the error of curve fitting is calculated by the ratio of the difference between predicted total mass and observed total mass to the observed total mass. The error averages about 7% with a maximum of 15%.

If the velocity profile is accurate, errors in Q or S will be linearly carried to R_{ia} or R_{fa} according to equation 3-21 and 3-25.

5.2.4 Summary of experimental errors

The potential average experimental errors are summarized in Table 5-1.

Table 5-1 Summary of average errors in this study

Error/Bias Source	m	u_*'	κ_a	S	Q	R_{ia}	R_{fa}
Curve fitting on velocity profile	5%	0	5%	5%	0	16%	10%
Cup anemometer calibration	3%	0	3%	3%	0	9%	6%
Sand surface change (max error)	3%	0	3%	3%	0	10%	6%
Estimation of velocity profile inside the saltation layer	0	0	0	Unknown	0	Unknown	Unknown
Reynolds stress measurement (max error)	0	5%	5%	0	0	11%	0
Spanwise variability of the sediment flux	0	0	0	25%	25%	25%	25%
Omitting the sand above trap stack	0	0	0	2%	2%	2%	2%
Curve fitting on sediment flux profile	0	0	0	7%	7%	7%	7%

Among all the variables, u_*' has the lowest potential error, while R_{ia} and R_{fa} have the highest. However, all of these errors are expected to be randomly distributed. If this is indeed the case, then much of the error will average out. The regression analyses between κ_a and S, Q, R_{ia} and R_{fa} indicate that the chances that these relationships happened by accident are smaller than 0.1% (with $p < 0.001$).

5.3 Implications

5.3.1 Implications for shear velocity

Many aeolian applications require estimating the shear velocity. At present, wind profile measurement and the Law of the Wall are still commonly used to derive shear velocity. However, this shear velocity will be possibly overestimated during aeolian saltation without considering the variability of κ_a. Here I will introduce a method to estimate "true" shear velocity by only using wind profile data and sediment transport data.

The experimental results show κ_a is the function of S_{25}. It is logical to use it to estimate κ_a and then the "true" shear velocity. However, the estimation of S_{25} requires the velocity profiles within the saltation layer, which is difficult to be measured directly. Using physical models (e.g. Li et al., 2004) to estimate the profile may introduce more uncertainty in estimating κ_a. On the other hand, the mass flux profile is easily measured by a stack of hose traps. If the concentration profile is highly correlated with the normalized mass flux (q) profile, then q is sufficient for the estimation of κ_a.

Regression analysis between S and q from all the traps of each run indicates a very strong linear relationship between S and q, with $R^2 = 0.94$ (Figure 5-1). Since q is linearly related to the total sediment transport rate Q, a similar relationship between S and Q is expected. To better represent the bulk effect of the sediment mass flux, Q, instead of q from each trap, is used for regression analysis with κ_a. There is a very strong negative linear relationship between Q and κ_a (Figure 5-2), which confirms the feasibility of replacing S by Q.

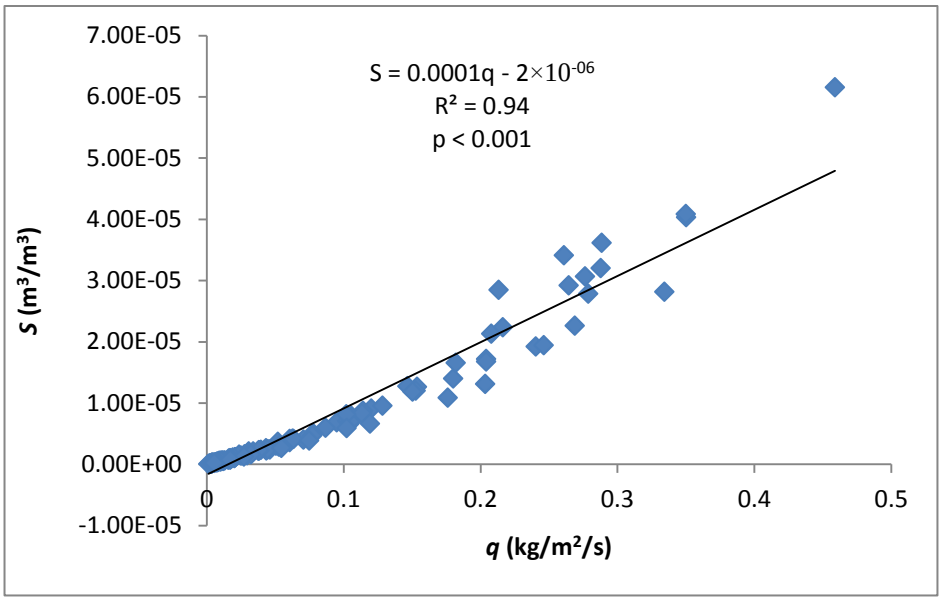

Figure 5-1 Results of regression analysis between *S* and *q*. Data are from Table 4-6 and Table 4-9.

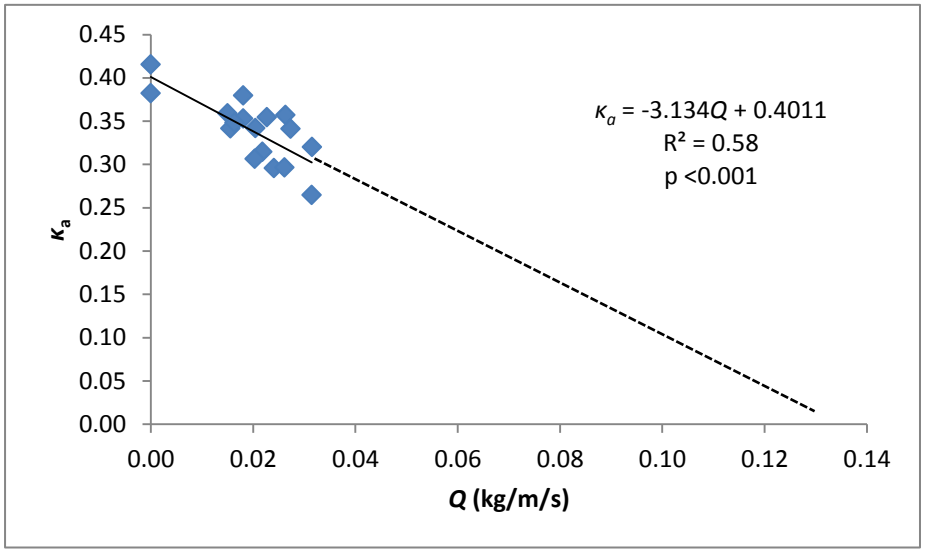

Figure 5-2 Results of regression analysis between Q and κ_a.

As Q and m are commonly reported in aeolian studies, κ_a and the predicted "true" shear velocity, u_*'', can be estimated using the following equation,

$$u_*'' = m\kappa_a = m(-3.134Q + 0.4011) \quad (5\text{-}1)$$

However, this relationship may be only valid within our measured Q range. In the case of fast Q, the value of κ_a is not realistic. For example, when Q is over 0.13 kg/m/s, from Figure 5-2, κ_a becomes negative. However, the smallest theoretical value of κ_a should be still positive because it is related to molecular path length when the stratified flow becomes laminar. This implies the true relationship between Q and κ_a is not linear.

Using equation 5-1, with observed Q data, the predicted "true" shear velocity, u_*'', was calculated. Regression analysis was performed to compare the predicted shear velocity u_*'' with estimates of u_*' from Reynolds stress measurements. The slope of the regression line was forced to cross (0, 0), and 10% error bars were plotted in Figure 5-3.

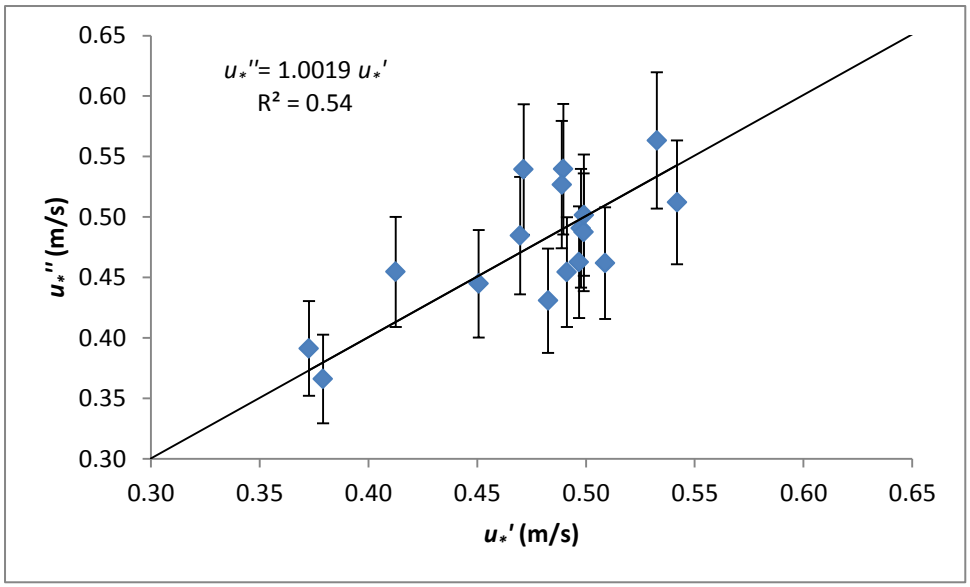

Figure 5-3 Results of regression analysis between u_*'' and u_*'.

The regression results indicate R^2 is 0.54, slope is 1.0019, which is very close to 1, and almost all the predicted values are within 10% of the error range. Therefore, with known Q and m, equation 5-1 can be used to provide reasonable estimates of the "true" shear velocity.

If using the canonical value of $\kappa = 0.4$, then a shear velocity without correction can be estimated using $u_* = 0.4m$. The ratios of u_* to u_*'' from sediment-laden runs were plotted against u_* in Figure 5-4.

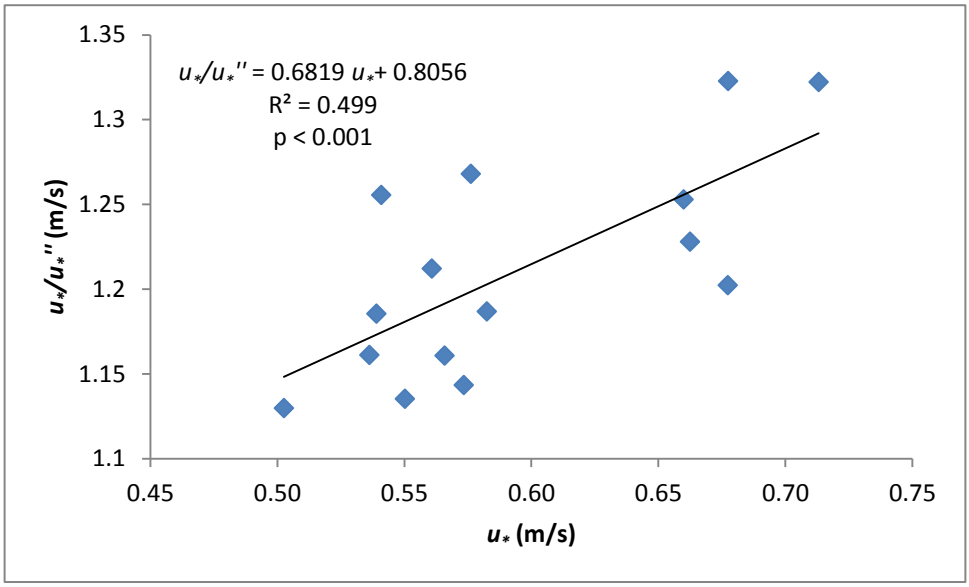

Figure 5-4 Results of regression analysis between u_*'' / u_* and uncorrected u_*.

Regression analysis indicates that u_*/u_*'' is proportional to u_*, the larger the u_*, the larger the u_*/u_*''. For example, there is about 15% overestimation when $u_* = 0.50$ m/s but this overestimation is doubled when $u_* = 0.72$ m/s. These results show that all the aeolian sediment experiments using $u_* = 0.4m$ instead of equation 5-1 have overestimated the shear velocity, especially when shear velocity is very fast. This makes sense because as u_* increases, so does Q, and this leads to a larger difference between κ and κ_a. Therefore, the validity of some classic

sediment transport models (e.g. Bagnold 1936, Lettau and Lettau, 1977) requires re-evaluation and the empirical constants in these models are likely underestimated, especially as Q or u_* increases.

5.3.2 Implications for sediment transport rate Q

Sediment transport rate, Q, is usually considered a function of u_*^3 (e.g. Bagnold, 1936; Kawamura, 1950; Lettau and Lettau, 1977). Traditionally, shear velocity is estimated from wind profiles and $\kappa = 0.4$. However, this study shows that the assumption of $\kappa = 0.4$ is not valid during aeolian saltation, and the κ_a is a function of Q as demonstrated in equation 5-1. Assuming a series of measured m values from 0.54 to 1.5 on a sandy surface with mean grain size of 0.297 mm, the simulated Q values with and without κ_a correction using Lettau and Lettau (1977) equation (equation 2-2) can be described in Figure 5-5. It appears that Q is a power function of m without κ_a correction and it appears as a quasi linear function of m with κ_a correction. Therefore, with the increase of m, the gap between these simulated transport rates also increases.

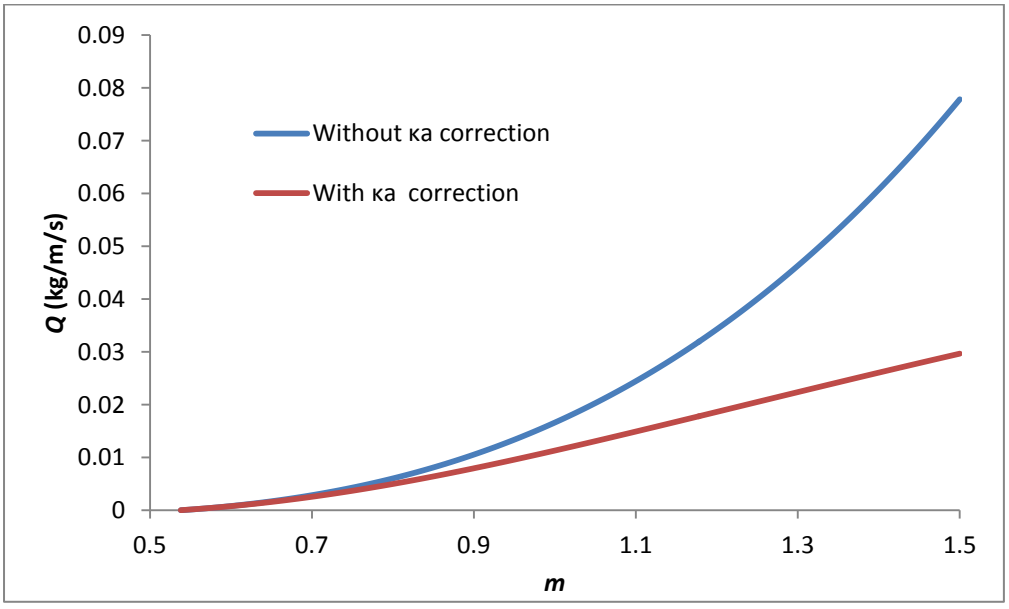

Figure 5-5 Simulated Q values with and without κ_a correction using equation 2-2.

5.3.3 Other implications

The experimental results indicate that κ_a ranges from 0.26 to 0.42, more than a 160% difference. The failure to account for κ_a variability will lead to substantial error in shear velocity estimation from the Law of the Wall. Besides the its potential influence on Q, as discussed in section 5.3.2, the error in shear velocity would also impact the estimates of apparent roughness length z_{0a} since it is a function of u_*^2 (e.g. Sherman, 1992; Sherman and Farrell, 2008). In other words, this research would affect all the sediment transport applications based on the shear velocity estimations using the Law of the Wall and velocity profiles. Empirically, this study will have broader impact on sediment beach and soil protection, dune stabilization, desertification assessment, coastal sediment budgets since these applications often require the prediction of sediment transport rate.

5.4 Limitations

The conclusions made from this study are only valid for a certain range of shear velocities and sediment transport rates. The inverse relationship between Q and κ_a suggests that a very fast transport rate will cause a very small or even negative κ_a. This indicates the true relationship is non-linear, of a nature that cannot be determined from the results of this experiment.

The sediment-laden experiment was conducted on dry, flat sand sheet with limited grain size range. The gravimetric moisture content was also very low (< 2%). If an in-situ environment is different, e.g. large grain size range, steep slope or wet surface, the conclusions may not be applicable.

If the grain size is as small as silt, the characteristics of the flow would be very different because the major sediment transport mode is suspension instead of saltation. Therefore stratification may not be prominent near the surface due to the absence of saltation layer. When

there is a surface slope, the sediment transport rate is a function of slope angle, which has been discussed by Bagnold (1973). In conditions where there is a wet surface, the threshold shear velocity increases dramatically, and the wet, entrained sediment would be "heavier" than the dry sediment, therefore, equation 5-1 should be also corrected for moisture content. These influences are beyond the scope of this research and will not be discussed in detail here.

5.5 Summary

The stratification theory seems to explain the variability of the apparent von Kármán parameter during aeolian saltation. The thermal stratification effect can be neglected compared to the sediment stratification effect.

Although there are errors in this experiment, it is unlikely that they are of a combined magnitude sufficient to invalidate the results. This view is supported by the regression analyses, which indicate it is not likely that the strong relationships between κ_a and S, Q and Richardson numbers occurred accidentally.

There is more than 60% difference in κ_a with and without aeolian saltation. This variability has substantial impact on all the applications using shear velocity obtained from velocity profile measurements. A method was proposed to estimate "true" shear velocity using velocity profile slope and sediment transport rate.

The results from this study may only be applicable for certain environments, e.g. flat, dry, sandy surfaces without extremely strong wind (with $u_*' > 0.6$ m/s). More research should be conducted in these fields.

6. SUMMARY AND CONCLUSIONS

The von Kármán constant, κ, is a well-known, universal constant of about 0.4, used to scale fluid mixing length in a turbulent boundary layer. It is commonly used in the Law of the Wall, which may be used to derive estimates of shear velocity. However, previous hydrodynamic studies indicate that there is an apparent change of κ in sediment-laden flows. This variable form of κ was termed the apparent von Kármán parameter, or κ_a, by Wright and Parker (2004). The variation of κ_a was explained by the energy loss for supporting the sediment suspension in the fluid, or by stratification effect from density gradient. The former is related to the mean grain size d, and the sediment concentration S, or, simply, the sediment transport rate Q. The latter is related to the air-sediment mixture density gradient, analogous to the concept of thermal stratification in atmospheric boundary layer, which can be quantified with the sedimentological gradient Richardson number R_i or flux Richardson number R_f , or their concentration weighted average values, R_{ia} and R_{fa}.

Field experiments were conducted on the northeast coast of Brazil near Jericoacoara. The purpose of the experiments was to examine the variability of apparent von Kármán parameter, κ_a, with and without aeolian saltation. Wind profile, "true" shear velocity and sediment flux profile data were collected to obtain the estimates of d, S, Q, R_{ia} *and* R_{fa}. After analyzing the experiment data, the following conclusions are drawn:

1) There is a substantial decrease of κ_a during aeolian saltation. The field experiment results show the lowest apparent value can be about 66% of the canonical value of 0.4. Under conditions with substantial aeolian transport, the Law of the Wall must be corrected using the apparent von Kármán parameter,

$$u = \frac{u_*'}{\kappa_a} \ln\left(\frac{z}{z_0}\right) \qquad (6\text{-}1)$$

In conditions without aeolian saltation, our results indicate that $\kappa_a = 0.399 = \kappa$.

2) There is not a statistically significant relationship between κ_a and d, maybe because of the small range of grain size at the study site or small sample size. Therefore, the supporting energy theory cannot be used here to explain the variability of κ_a.

3) There is a strong relationship between κ_a and S_{25} (bulk, volumetric sediment concentration at $0 < z < 0.25$ m, or from bottom trap), and between κ_a and Q as,

$$\kappa_a = -2088.4 S_{25} + 0.3964 \qquad R^2 = 0.70 \qquad (6\text{-}2)$$

$$\kappa_a = -3.134 Q + 0.4011 \qquad R^2 = 0.58 \qquad (6\text{-}3)$$

4) A strong relationship was found between κ_a and R_i or between κ_a and R_f in the lower part of the saltation layer. Regression analysis also shows that there is a strong relationship between κ_a and R_{ia} and between κ_a and R_{fa}:

$$\kappa_a / \kappa = 1 - 31.270 R_{ia} \qquad R^2 = 0.66 \qquad (6\text{-}4)$$

$$\kappa_a / \kappa = 1 - 2.7877 R_{fa} \qquad R^2 = 0.67 \qquad (6\text{-}5)$$

The strong relationships confirm the applicability of stratification theory in aeolian saltation.

Shear velocity estimates derived from uncorrected Law of the Wall could be significantly overestimated, under conditions with substantial saltation. This would affect many aeolian applications. For example, a 60% underestimation in κ_a would cause 67% overestimation in u_*, which leads to 463% over-prediction in sediment transport rate using Bagnold's (1936) model and 278% overestimation in apparent roughness length using the model by Sherman et al. (1992). To compensate this potential overestimation, it is necessary to re-evaluate the empirical constants in these models.

There are, inevitably, experimental errors due to imperfect design (no wind measurement in the saltation layer), instrument accuracy (instrument calibration and voltage loss in the cable) and insufficient knowledge in saltation mechanism (spanwise transport variability). However, except for d, most of the regression analyses with κ_a are statistically significant at 99.9% confidence level, indicating the chances to obtain these results by accident are very small.

The presence of wind-blown sand alters the wind. Therefore the Law of the Wall requires modification in the presence of saltating sand. This finding should influence the future theoretical aeolian studies. With the implications on sediment transport models, this research also has broader impact for practical applications considering beach and soil protection, dune stabilization, desertification assessment, coastal sediment budgets, and other related environmental challenges.

REFERENCES

Adams, C. E., and G. L. J. Weatherly. 1981. Some effects of suspended sediment stratification on an oceanic bottom boundary layer. *Journal of Geophysical Research* 86 (C5):4161-4172.

Anderson, R., and P. Haff. 1991. Wind modification and bed response during saltation of sand in air. *Acta Mechanica* 1:21-52.

Andreas, E., K. Claffey, R. Jordan, C. Fairall, P. Guest, P. Persson, and A. Grachev. 2006. Evaluations of the von Kármán constant in the atmospheric surface layer. *Journal of Fluid Mechanics* 559:117-149.

Bagnold, R. A. 1936. The movement of desert sand. Proceedings of the Royal Society of London. Series A, *Mathematical and Physical Sciences* 157 (892):594-620.

Bagnold, R. A. 1973. The nature of saltation and "bed-load" transport in water, *Proceedings of the Royal Society of London*, 332: 473-504.

Bauer, B., C. Houser, and W. Nickling. 2004. Analysis of velocity profile measurements from wind-tunnel experiments with saltation. *Geomorphology* 59 (1-4):81-98.

Bennett, S., J. Bridge, and J. Best. 1998. Fluid and sediment dynamics of upper stage plane beds. *Journal of Geophysical Research* 103 (C1):1239-1274.

Best, J., S. Bennett, J. Bridge, and M. Leeder. 1997. Turbulence modulation and particle velocities over flat sand beds at low transport rates. *Journal of Hydraulic Engineering* 123 (12):1118-1129.

Blott, S., and K. Pye. 2001. GRADISTAT: a grain size distribution and statistics package for the analysis of unconsolidated sediments. *Earth Surface Processes and Landforms* 26 (11):1237-1248.

Brunel, J. 1989. Estimation of sensible heat flux from measurements of surface radiative temperature and air temperature at two meters: application to determine actual evaporation rate. *Agricultural and Forest Meteorology* 46 (3):179-191.

Businger, J., J. Wyngaard, Y. Izumi, and E. Bradley. 1971. Flux-profile relationships in the atmospheric surface layer. *Journal of the Atmospheric Sciences* 28 (2):181-189.

Chen, W., and D. Fryrear. 2001. Aerodynamic and geometric diameters of airborne particles. *Journal of Sedimentary Research* 71 (3):365.

Chien, N., and Z. Wan. 1999. *Mechanics of sediment transport*. Reston, VA (US): American Society of Civil Engineers.

Coleman, N. L. 1981. Velocity Profiles with Suspended Sediment. *Journal of Hydraulic Research* 19 (3).

Coleman, N. L. 1986. Effects of suspended sediment on the open-channel velocity distribution. *Water Resources Research* 22 (10):1377-1384.

Cornelis, W. M., and D. Gabriels. 2003. The effect of surface moisture on the entrainment of dune sand by wind: an evaluation of selected models. *Sedimentology* 50 (4):771-790.

Einstein, H., and N. Chien. 1955. Effects of heavy sediment concentration near the bed on velocity and sediment distribution. Sediment Series No. 8. Institute of Engineering Research, University of California, Berkeley.

Elata, C., and A. T. Ippen. 1961. The dynamics of open channel flow with suspensions of neutrally buoyant particles. Technical Report No. 45. Hydrodynamics Lab, MIT.

Ellis, J., B. Li, E. Farrell, and D. Sherman. 2009. Protocols for characterizing aeolian mass-flux profiles. *Aeolian Research* 1 (1-2):19-26.

Farber, K. 1986. Investigations of particle motions in turbulent flow. In *Transport of Suspended Solids in Open Channels*, ed. W. Bechteler, 33-36. Rotterdam: Balkema.

Frenzen, P., and C. Vogel. 1995. A further note "on the magnitude and apparent range of variation of the von Kármán constant". *Boundary-Layer Meteorology* 75 (3):315-317.

Frenzen, P., and C. A. Vogel. 1995. On the magnitude and apparent range of variation of the von Kármán constant in the atmospheric surface layer. *Boundary-Layer Meterology* 72:371-392.

Gares, P., R. Davidson-Arnott, B. Bauer, D. Sherman, R. Carter, D. Jackson, and K. Nordstrom. 1996. Alongshore variations in aeolian sediment transport: Carrick Finn Strand, Ireland. *Journal of Coastal Research* 12 (3):673-682.

Gelfenbaum, G., and J. Smith. 1986. Experimental evaluation of a generalized suspended-sediment transport theory. *Shelf Sands and Sandstones*:133-144.

Gilbert, G. 1914. *The transportation of debris by running water*, Prof. Paper No. 86, 263. Washington, DC: US Geological Survey.

Graf, W., and M. Cellino. 2002. Suspension flows in open channels; experimental study. *Journal of Hydraulic Research* 40 (4):435-447.

Greeley, R., and J. D. Iversen. 1985. *Wind as a geological process on Earth, Mars, Venus and Titan.* New York: Cambridge University Press.

Gust, G., and J. B. Southard. 1983. Effects of weak bed load on the universal law of the wall. *Journal of Geophysical Research* 88 (C10):5939-5952.

Herrmann, M., and O. Madsen. 2007. Effect of stratification due to suspended sand on velocity and concentration distribution in unidirectional flows. *Journal of Geophysical Research* 112 (C2):C02006.

Högström, U. 1988. Non-dimensional wind and temperature profiles in the atmospheric surface layer: A re-evaluation. *Boundary-Layer Meteorology* 42 (1):55-78.

Howard, L. 1961. Note on a paper of John W. Miles. *Journal of Fluid Mechanics* 10 (04):509-512.

Jackson, N., D. Sherman, P. Hesp, A. Klein, and K. Nordstrom. 2006. Small-Scale Spatial Variations in Aeolian Sediment Transport on a Fine-Sand Beach. *Journal of Coastal Research* SI 39:379-383.

Jimenez, J., L. Maia, J. Serra, and J. Morais. 2002. Aeolian dune migration along the Cear á coast, north-eastern Brazil. *Sedimentology* 46 (4):689-701.

Kaimal, J., and J. Finnigan. 1994. *Atmospheric boundary layer flows: Their structure and measurement*. New York: Oxford Univ. Press,.

Kalinske, A., and C. Hsia. 1945. Study of transportation of fine sediments by flowing water. In Bulletin No. 29, 32: University of Iowa, Studies in Engineering.

Kawamura, R. 1951. Study of sand movement by wind. In *Reports of Physical Sciences Research*: Institute of Tokyo University. 5 (3-4):95-112.

Keulegan, G. 1938. Laws of turbulent flow in open channels. *Journal of Research of the National Bureau of Standards* 21:707-741.

Kobayashi, A. S., and W. L. Moss. 1969. Stress intensity magnification factors for surface-flawed tension plate and notched round tension bar. *Proceedings of second internat conference on fracture*, Brighton, England.

Lees, B. 1981. Relationship between eddy viscosity of seawater and eddy diffusivity of suspended particles. *Geo-Marine Letters* 1 (3):249-254.

Lettau, H., and B. Davidson. 1957. *Exploring the Atmosphere's First Mile: Instrumentation and data evaluation*. New York: Symposium Publications Division, Pergamon Press.

Lettau, K., and H. Lettau. 1977. Experimental and micrometeorological field studies of dune migration. In *Exploring the World's Driest Climate*. , eds. K. Lettau and H. Lettau, 110-147: Center for Climatic Research, University of Wisconsin-Madison, IES Report 101.

Li, Z., J. Ni, and C. Mendoza. 2004. An analytic expression for wind-velocity profile within the saltation layer. *Geomorphology* 60 (3-4):359-369.

Maia, L., G. Freire, and L. Lacerda. 2005. Accelerated dune migration and aeolian transport during El Nino events along the NE Brazilian coast. *Journal of Coastal Research* 21 (6):1121-1126.

McEwan, I. 1993. Bagnold's kink: a physical property of a wind profile modified by blown sand. *Earth Surface Processes and Landforms* 18:145-156.

McLean, S. 1992. On the calculation of suspended load for noncohesive sediments. *Journal of Geophysical Research-Oceans* 97 (C4):5759-5770.

Monin, A., and A. Obukhov. 1954. Basic laws of turbulent mixing in the ground layer of the atmosphere. *Tr. Geofiz. Inst. Akad. Nauk SSSR* 151:163-187.

Monin, A., and A. Yaglom. 1971. *Statistical Fluid Mechanics: Mechanics of Turbulence*. Cambridge: MIT Press.

Muste, M. 2002. Sources of bias errors in flume experiments on suspended-sediment transport *Journal of Hydraulic Research* 40 (6):695-708.

Namikas, S. 2002. A floating-element drag plate for direct measurement of bed shear stress during eolian transport. *Journal of Sedimentary Research* 72 (2):328.

Namikas, S. 2003. Field measurement and numerical modelling of aeolian mass flux distributions on a sandy beach. *Sedimentology* 50 (2):303-326.

Nemoto, M., and K. Nishumura. 2001. Direct measurement of shear stress during snow saltation. *Boundary-Layer Meteorology* 100 (1):149-170.

Nezu, I., and R. Azuma. 2004. Turblulence characteristics and interaction between particles and fluid in particle-laden open channel flows. *Journal of Hydraulic Engineering* 130 (10):988-1001.

Nikuradse, J. 1932. *Laws of turbulent flow in smooth pipes (English translation)*. NASA TT F-10 (1966).

Nouh, M. 1989. The von-Kármán coefficient in sediment laden flow. *Journal of Hydraulic Research* 27 (4):477-499.

Oke, T. 1978. *Boundary Layer Climates*. London: Methuen & Co Ltd.

Owen, P. 1964. Saltation of uniform grains in air. *Journal of Fluid Mechanics* 20 (02):225-242.

Owen, P. 1980. The physics of sand movement. In Lecture Notes, Workshop on Physics of Flow in Desert, 84. Trieste: International Centre for Theoretical Physics.

Owen, P., and D. Gillette. 1985. Wind tunnel constraint on saltation. In *Proceedings of the International Workshop on the Physics of Blown Sand, Memoir No. 8*, eds. O. E. Barndorff-Neilsen, J.-T. Møller, K. R. Rasmussen and B. B. Willetts, 253-269: University of Aarhus, Denmark.

Reynolds, O. 1894. On the dynamical theory of incompressible viscous flows and the determination of the criterion. *Philosophical Transactions of the Royal Society of London Series A* 186,123-161.

Pardyjak, E., P. Monti, and H. Fernando. 2002. Flux Richardson number measurements in stable atmospheric shear flows. *Journal of Fluid Mechanics* 459:307-316.

Pease, P., S. Lecce, P. Gares, and M. Lange. 2002. Suggestions for Low-Cost Equipment for Physical Geography II: Field Equipment. *Journal of Geography* 101 (5):199-206.

Prandtl, L. 1925. *Bericht über Untersuchungen zur ausgebildeten Turbulenz, Zs. agnew. Math. Mech* 5:136-139.

Richardson, L. F. 1922. *Weather Prediction by Numerical Process*. Cambridge: Cambridge University Press.

Ritter, D. F., R. C. Kochel, and J. R. Miller. 2002. *Process Geomorphology*. 4th Edition ed: McGraw-Hill

Rose, C., and P. Thorne. 2001. Measurements of suspended sediment transport parameters in a tidal estuary. *Continental Shelf Research* 21 (15):1551-1575.

Rouse, H. 1936. Discharge characteristics of the free overfall. *Civil Engineering* 6 (4):257-260.

Shao, Y. 2000. *Physics and Modelling of Wind Erosion*: Kluwer Academic Boston.

Shao, Y., and A. Li. 1999. Numerical modelling of saltation in the atmospheric surface layer. *Boundary-Layer Meteorology* 91 (2):199-225.

Sheppard, P. 1947. The aerodynamic drag of the earth's surface and the value of von Karman's constant in the lower atmosphere. *Proceedings of the Royal Society of London. Series A, Mathematical and Physical Sciences*:208-222.

Sherman, D. 1992. An equilibrium relationship for shear velocity and apparent roughness lenght in aeolian saltation. *Geomorphology* 5 (3-5):419-431.

Sherman, D., and E. Farrell. 2008. Aerodynamic roughness lengths over movable beds: Comparison of wind tunnel and field data. *Journal of Geophysical Research-Earth Surface* 113 (F2):F02S08.

Sherman, D. J., D. W. T. Jackson, S. L. Namikas, and J. Wang. 1998. Wind-blown sand on beaches: an evaluation of models. *Geomorphology* 22 (2):113-133.

Soulsby, R., A. Salkield, R. Haine, and B. Wainwright. 1986. Observations of the turbulent fluxes of suspended sand near the sea-bed. In *Transport of Suspended Solids in Open Channels*, ed. W. Bechteler, 183-186. Rotterdam: Balkema.

Stull, R. 1988. *An introduction to boundary layer meteorology*: Norwell, MA: Kluwer Academic Publishers.

Styles, R., and S. Glenn. 2000. Modeling stratified wave and current bottom boundary layers on the continental shelf. *Journal of Geophysical Research* 105 (C10):24,119-24,139.

Thom, A. 1976. Momentum, mass and heat exchange of plant communities. In *Vegetation and the Atmosphere*, ed. J. L. Monteith, 57-109. New York: Academic Press.

van Boxel, J. H., G. Sterk, and S. M. Arens. 2004. Sonic anemometers in aeolian sediment transport research. *Geomorphology* 59 (1):131-147.

van Rijn, L. C. 1985. Sediment transport. Delft, Netherland: Delft Hydraulic Laboratory.

Vanoni, V. A., and G. N. Nomicos. 1960. Resistant properties of sediment-laden streams. *Transactions of the American Society of Civil Engineers* 125:1140-1175.

von Kármán, T. 1930. *Mechanische Ähnlichkeit und Turbulenz*. Göttingen: Nachrichten der Akademie der Wissenschaften.

Walker, I. 2005. Physical and logistical considerations of using ultrasonic anemometers in aeolian sediment transport research. *Geomorphology* 68 (1-2):57-76.

Walker, I., and W. Nickling. 2003. Simulation and measurement of surface shear stress over isolated and closely spaced transverse dunes in a wind tunnel. *Earth Surface Processes and Landforms* 28 (10):1111-1124.

Wang, Z., and P. Larsen. 1994. Turbulent structure of water and clay suspensions with bed load. *Journal of Hydraulic Engineering* 120 (5):577-600.

Werner, B. 1990. A steady-state model of wind-blown sand transport. *Journal of Geology* 98 (1):1-17.

Wright, S. and G. Parker, 2004. Density stratification effects in sand-bed rivers. *Journal of Hydraulic Engineering* 130:783-795.

Zhang, W., Y. Wang, and S. Lee. 2007. Two-phase measurements of wind and saltating sand in an atmospheric boundary layer. *Geomorphology* 88 (1-2):109-119.

APPENDIX

VARIABILITY OF THE APPARENT VON KÁRMÁN PARAMETER DURING AEOLIAN SALTATION[1]

Bailiang Li[*], Douglas J. Sherman[*], Eugene J. Farrell[*], Jean T. Ellis[#]

* Department of Geography,
Texas A&M University,
College Station,
TX 77843-3147

Department of Geography,
Marine Sciences Program,
University of South Carolina
Columbia, SC 29208

Abstract

The variability of the apparent von Kármán parameter κ_a during aeolian saltation was evaluated in a field experiment at Jericoacoara, Brazil. To test this variability, velocity profiles, Reynolds stress and sand transport data were gathered and analyzed. We used 15 data sets with sand-laden airflow and 2 runs with clear airflow. Results indicated an inverse linear relationship between κ_a and bulk, gravimetric sand concentration (R^2 = 0.746) and sand transport rate (R^2 = 0.577). We found values of κ_a as low as 0.26. This means that using the von Kármán constant, κ (0.40) rather than the variable κ_a to estimate shear velocity based on the slope of the velocity profile will lead to over estimation of shear velocity, averaging about 20% in this study. This, in turn, produces an over estimation of wind-blown sand transport rates based on models that have terms with shear velocity cubed.

[1] This paper has been published in *Geophysical Research Letters*, reproduced with permission of American Geophysical Union. Full citation: Li, B., D. J. Sherman, E. J. Farrell, and J. T. Ellis (2010), Variability of the apparent von Kármán parameter during aeolian saltation, *Geophys. Res. Lett.*, 37, L15404, doi:10.1029/2010GL044068.

1. Introduction

Understanding the mechanics of sediment transport and the development of transport models have been central themes in aeolian geomorphology for almost a century [*Hobbs*, 1917; *Bagnold*, 1936; *Ellis et al.*, 2009]. Despite decades of detailed field and laboratory experimentation, there remains relatively poor agreement between observed and predicted rates of sand transport by wind, especially for natural environments [e.g., *Sherman et al*., 1998; *Dong et al.*, 2003; or *Bauer et al*., 2009]. Almost all physics-based models predict sand transport rates as a function of the third power of shear velocity [e.g., *Sørensen*, 2004]. Therefore, small errors in estimations of shear velocity may lead to large errors in predicted transport rates. In wind tunnel and field experiments, shear velocity, u_*, is commonly derived as the product of the slope of a measured velocity profile *du/ln(dz)* and the von Kármán constant, κ. Wind-blown sand studies, whether conducted in the laboratory or in the field generally assume that κ is constant, with typical values of 0.40 or 0.41. Conversely, hydrodynamic research indicates that this "constant" appears to vary in the presence of suspended or bed load sediment transport. For example, values of κ less than 0.20 are reported by *Einstein and Chien* [1955], which would cause errors in transport predictions, *ceteris paribus*, to exceed 800%. For application in sand-bedded rivers, Wright and Parker (2004) introduce the concept of a variable, *apparent von Kármán parameter* to describe this phenomenon. There have been no attempts, to the authors' knowledge, to evaluate the stability of the von Kármán constant (or the apparent von Kármán parameter) in the presence of wind-blown sand. Here we report the results of field experiments designed to detect and characterize apparent changes in the von Kármán constant caused by the presence of saltating sand grains.

2. Background

The importance of understanding the stability or variability of the von Kármán constant stems from a few relationships that are critical to the study of wind-blown sand. Since the foundational work of *Bagnold* [1936], almost every aeolian transport equation assumes *Q*, the mass transport rate is a function of shear velocity, u_*^3. *Lettau and Lettau's* [1977] model, among others, illustrates this relationship:

$$Q = C(u_* - u_{*t})u_*^2 \quad (1)$$

where *C* is an empirical constant related to grain size and u_{*t} is the threshold shear velocity. *Lettau and Lettau* [1977] quantify *C* using:

$$C = c\sqrt{\frac{d}{D}}\frac{\rho}{g} \quad (2)$$

Here, *c* is an empirical constant, commonly set as 4.2, although some higher values have been reported [*Wippermann and Gross*, 1986; *Liu et al.*, 2006], *g* is gravity acceleration (9.81 m/s^2), *d* is mean grain diameter, ρ is air density (1.201 kg/m^3 at 20 ℃), and *D* is a reference grain diameter of 0.25 mm.

For a steady state, homogeneous turbulent boundary layer there is a constant stress layer within which:

$$\tau = -\rho\overline{u'w'} = \rho K\frac{\partial u_z}{\partial z} = \rho u_*^2 \quad (3)$$

Here, τ is shear stress, u' and w' are the instantaneous horizontal and vertical velocity fluctuation components, *K* is eddy viscosity, u_z is mean wind speed at elevation *z*. The term $-\rho\overline{u'w'}$ represents the Reynolds stresses. From Prandtl's mixing length theory:

$$K = l^2\left|\frac{\partial u_z}{\partial z}\right| \quad (4)$$

where l is a mixing length scaled against elevation by the von Kármán constant: $l = \kappa z$. Equations 3 and 4 can be combined to solve for shear velocity:

$$u_* = \kappa z \frac{\partial u_z}{\partial z} \quad (5)$$

This relationship is formalized in the Law of the Wall to describe the velocity distribution in the inner turbulent layer:

$$u_z = \frac{u_*}{\kappa} \ln\left(\frac{z}{z_0}\right) \quad (6)$$

where z_0 is the roughness length.

Based upon observations of wind speeds and the Law of the Wall, shear velocity can be estimated using $u_* = m\kappa$, where m is the slope of the least squares line fit to the velocity profile by linear regression of ln(z) (independent variable) against u_z (dependent variable). If the von Kármán constant varies in this application, as suggested by analogy to fluvial systems, there will be direct impacts on estimates of shear velocity. Roughness length can be estimated using $z_o = e^{-(b/m)}$ (where b is the intercept of the least squares line) and is also recognized to vary in the presence of saltating grains as a function of u_*^2 [*Owen*, 1964; *Sherman and Farrell*, 2008]. Saltating grains increase the roughness length, thereby increasing m and decreasing b.

Studies of the von Kármán constant in fluids, including water in pipes [*Nikuradse*, 1932; *McKeon et al.*, 2004], open channels [*Keulegan*, 1938], and air in the atmospheric surface layer [*Frenzen and Vogel*, 1995a,b] indicated that the von Kármán constant varies over a range of 0.36-0.43. The Glossary of Meteorology [*Glickman*, 2000] indicates $\kappa = 0.40 \pm 0.01$, and a recent atmospheric experiment over polar sea ice confirmed κ within the range of 0.387 ± 0.003 [*Andreas et al.*, 2006]. In studies of blowing sand, it is commonly assumed that $\kappa = 0.40$.

Studies of hydrodynamic systems indicate that the "log law" is valid in the inner turbulent region of the boundary layer but that the von Kármán constant can vary with sediment load. Several studies found that as sediment concentrations increase, the von Kármán constant decreases [*Einstein and Chien*, 1955; *Vanoni and Nomicos*, 1960; *Elata and Ippen*, 1961; *Best et al.,* 1997; *Bennett et al.*, 1998; *Nezu and Azuma*, 2004], with values of k ranging from 0.168 to 0.427. These findings compromise assumptions about the apparent constancy of κ. We refer to apparent constancy because the physical circumstances are not quite that simple.

Smith and McLean [1977] argued that sand-laden water flows could be treated as stratified systems. The changes in velocity gradient induced by the density gradient manifest an apparent variability of the von Kármán constant that can be corrected using a flux Richardson Number. *Adams and Weatherly* [1981] used the flux Richardson Number and the Monin-Obukov length scale (following the atmospheric thermal gradient analogy) to modify the Law of the Wall to allow the von Kármán constant to remain set at 0.40 while still reproducing sediment-influenced velocity profiles. They introduced the concept of the "modified (reduced) von Kármán constant" that scales with the flux Richardson Number and that should replace $\kappa = 0.40$ in the Law of the Wall and when estimating u_* from velocity profiles. *Adams and Weatherly* [1981] note that failure to account for the effects of sediments in the fluid can, therefore, lead to overestimation of shear velocity. *Wright and Parker* [2004, p. 783] in a similar vein, define an "apparent von Kármán parameter, κ_a" for use in modeling the effects of near-bed grain concentrations in sand-bed rivers:

$$\frac{1}{\kappa_a} = \frac{d\left(u / u_*'\right)}{d\left(\ln z\right)} = \frac{m}{u_*'} \qquad (7)$$

where u_*' is the "true" shear velocity. For flows without sediments, the apparent von Kármán parameter equals the von Kármán constant: $u_*' = m\kappa_a = m\kappa = u_*$. During periods of transport, the

presence of sediments in the flow reduces the efficiency of turbulent mixing, i.e., there is a reduction in K, so that $l < \kappa z$. If this is the case, κ_a replaces κ for estimating u_*': $u_*' = m\kappa_a \neq m\kappa = u_*$. It is the variability of κ_a during aeolian saltation that we aim to assess with this research.

In order to evaluate κ_a, the velocity gradient m and "true" shear velocity u_*' must be known (from Equation 7). Measuring velocity profiles is straight-forward, and a profile-independent estimate of u_*' may be obtained using a Reynolds stress, τ, approach.

With advances in instrumentation (e.g. thermal and ultrasonic anemometry) it is possible to make direct estimates of the local instantaneous Reynolds' shear stress by averaging the product of the fluctuating components of the horizontal and vertical velocities [*van Boxel*, 2004]. Therefore, estimates of the "true" shear velocity, u_*', can be obtained from Equation 3.

3. Study Site

Field experiments were conducted in October and November, 2008 at two sites in Jericoacoara, Ceará, Brazil. The first site was located on an intertidal sand flat. This site was used for "clear air" studies because the wet sands remained immobile with wind speeds of the order of 10 m/s, and there was a nearly horizontal, unobstructed fetch of more than 200 m upwind of the instrument location.

The second site was at the down-wind end of a sandy deflation plain, bounded by semi-parallel ridges that are the remnants of a migrating parabolic dune. The fetch distance exceeded 100 m, and the distances between the ridges was approximately 50 m where the instruments were located.

All data were gathered late enough in the afternoon that sand surface and air temperatures were similar. The relatively small temperature gradients and the fast wind speeds minimized concerns about non-neutrally buoyant boundary layer conditions. Scaling analysis using the Monin-Obuhkov length scale indicates near neutral conditions.

4. Experimental Design

The fluctuating velocity components, u' and w', were measured with an ultrasonic anemometer (R.M.Young 81000), with an internal sample rate of 160 Hz and 32 Hz output rate. *Van Boxel et al.* [2004] suggested using a sample rate of at least 20 Hz for an instrument located below 1 m elevation if the wind velocity is 10 m/s and the sampling duration period time should be at least 2 minutes to keep the variance losses of Reynolds stress less than 5%. To control accuracy, the ultrasonic anemometer was mounted at 1 m above the bed and the sampling durations were 120 s or longer (Table 1).

Table 1. Results from experiments; "-" means no data, not required for clear air study. R^2 is coefficient of determination from the log-linear curve fit to the velocity profile.

Run	Date	T (s)	d (mm)	u_*' (m/s)	u_* (m/s)	z_0 (mm)	K_a	R^2	p	Q (kg/m/s)	S_{25} (kg/kg)
1	10/22	120	0.30	0.54	0.68	3.400	0.320	0.991	0.0043	3.15E-02	0.1319
2	10/22	180	0.22	0.49	0.66	3.799	0.296	0.988	0.0055	2.40E-02	0.1226
3	10/22	180	0.22	0.47	0.71	4.185	0.264	0.992	0.0035	3.15E-02	0.1829
4	10/22	213	0.23	0.53	0.68	4.553	0.315	0.991	0.0043	2.18E-02	0.1264
5	10/24	170	0.30	0.49	0.66	2.806	0.296	0.995	0.0024	2.61E-02	0.1194
6	10/24	240	0.29	0.50	0.58	2.059	0.342	0.989	0.0052	2.04E-02	0.0908
7	10/24	240	0.28	0.50	0.57	1.806	0.353	0.993	0.0031	1.80E-02	0.0837
8	10/24	240	0.28	0.47	0.55	1.463	0.341	0.996	0.0020	1.56E-02	0.0644
9	10/24	240	0.30	0.45	0.50	1.054	0.359	0.986	0.0068	1.50E-02	0.0586
10	10/24	240	0.30	0.51	0.54	1.170	0.380	0.994	0.0028	1.81E-02	0.0757
11	10/26	240	0.25	0.48	0.54	2.131	0.357	0.997	0.0016	2.63E-02	0.0996
12	10/26	300	0.27	0.41	0.54	2.777	0.306	0.993	0.0034	2.03E-02	0.0912
13	10/30	240	0.33	0.50	0.56	0.836	0.354	1.000	0.0029	2.27E-02	0.0753
14	10/30	299	0.43	0.50	0.57	0.958	0.348	1.000	0.0085	1.64E-02	0.0373
15	10/30	240	0.44	0.49	0.58	0.897	0.341	1.000	0.0035	2.73E-02	0.0554
16	11/1	612	-	0.37	0.39	0.022	0.382	0.999	0.0172	-	-
17	11/1	644	-	0.38	0.37	0.014	0.415	1.000	0.0117	-	-

These measurements allowed us to solve Equation 3 for u_*'. Sampling was at 96 Hz and the data were smoothed to 32 Hz. For wind speed measurements at multiple elevations we used Gill type, 3-cup anemometers. Sampling was at 96 Hz and the data were smoothed to 4 Hz. These anemometers were deployed in two configurations. For Runs 1 through 12 there were vertical arrays of four anemometers at elevations of 0.25, 0.50, 0.75, and 1.00 m. For Runs 13 through 17 there were three anemometers at elevations of 0.25, 0.75, and 1.00 m. We used log-linear curve fitting to obtain velocity profiles (slope m and intercept b). These measurements, together with u_*' obtained with Equation 3, allow us to solve for $\kappa_a = u_*'/m$ as well as $z_0 = \exp(-b/m)$.

To measure sediment transport rates and concentrations, we deployed vertical arrays of eight hose-style traps [*Pease et al.*, 2002], with horizontal openings of 0.10 m and, from the surface up, vertical openings 0.025, 0.025, 0.050, 0.050, 0.050, 0.100, 0.100, and 0.100 m. After returning from the field, sand samples were dry-sieved at 0.25 φ intervals.

5. Results

We obtained 17 data sets suitable for assessment of the apparent von Kármán parameter: 15 with sand transport and 2 under "clear air" conditions. For these runs, the best-fit velocity profiles, based on linear regression, had R^2 values greater than 0.985 with p values all less than 0.02. From the data we obtained estimates of mean grain diameter, the slope of the log-linear velocity profile, saltation-enhanced (apparent) roughness length, shear velocity (assuming κ = 0.40) and "true" shear velocity, and the apparent von Kármán parameter. These results are summarized in Table 1.

We first compared shear velocity estimates obtained from the Reynolds stresses (Equation 3) and the velocity profiles (Equation 6) in two "clear air" samples where there was no sand transport (runs 16 and 17). For these runs, the "true" shear velocity u_*' estimates are 0.373

m/s and 0.379 m/s, while the values of u_* derived from velocity profile analyses were 0.390 m/s and 0.365 m/s, or about 7% different. The corresponding κ_a values are 0.382 and 0.415, close to the canonical value of 0.40 for κ. Indeed, if we average the two estimates of κ_a, we obtain a "best" estimate of 0.399. For conditions with sand transport, we derived estimates of κ_a using Equation 7. Our results indicated that κ_a varied from 0.264 to 0.380 for sand-laden flows.

Sediment transport rates, Q (kg/m/s), were derived from the sand mass, M, collected from the eight traps, normalized by trap stack width W (0.1 m) and run duration T,

$$Q = \frac{M}{WT} \tag{8}$$

To represent the near-bed conditions, where effects of stratification should be greatest [*Wright and Parker*, 2004], we define the bulk, gravimetric sand concentration S_{25} (kg/kg) using data from our lowest 0.025 m (25 mm) high trap:

$$S_{25} = \frac{M_{25}}{(\rho V_{25} + M_{25})} \tag{9}$$

where M_{25} is the sand mass (from the 25 mm bottom trap), and V_{25} is the volume of air passing through that trap, estimated from integration of the velocity profile,

$$V_{25} = WT\int_{z_0}^{z_b} u_z dz = mW[z_b \ln z_b - z_0 \ln z_0 - (1 + \ln z_0)(z_b - z_0)] \tag{10}$$

where, z_b is 25 mm, the height of the bottom trap. The values of Q and S_{25} for each run are listed in Table 1.

The apparent roughness length and the apparent von Kármán parameter should vary with changes in sand concentration and, presumably, with the sand transport rate. Regression analysis indicated that z_0 increases with $u_{*'}^2$ ($R^2 = 0.26$, $p < 0.05$). However, changes in z_0 are fully represented in the velocity profile data used to estimate m and b, and, therefore, cannot account for the measured disparities between u_* and $u_{*'}$. That leaves only κ_a as a compensating variable,

and we tested its dependence on sand concentration and transport rate using linear regression (Figure 1). Multiple curves were fit to assess the most applicable regression model. Linear regression produced the highest values of R^2 for both Q (0.577) and S_{25} (0.746) (c.f. Table 2). Because the apparent von Kármán parameter should match the von Kármán constant with no blowing sand, we also tested the relationships after forcing the regression line intercept to be (0, 0.399) (c.f. Table 2), based on the average κ_a from the clear air studies (Runs 16-17). All R^2 values are statistically significant at 99.9% confidence level ($p < 0.001$). The forced regression results allow prediction of the apparent von Kármán parameter based on measurements of sand transport rates or bulk, gravimetric sand concentrations:

$$\kappa_a = -3.028Q + 0.399 \qquad (11)$$

$$\kappa_a = -0.705S_{25} + 0.399 \qquad (12)$$

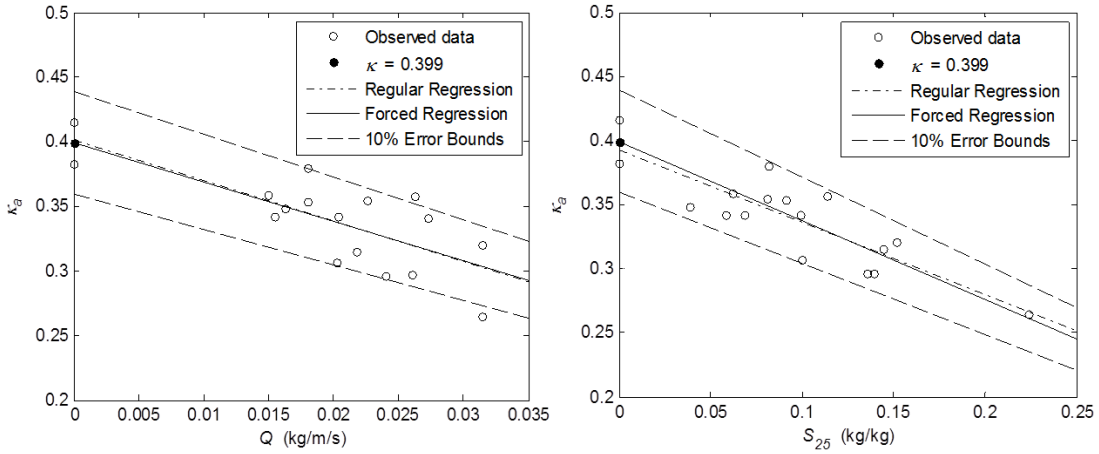

Figure 1. Regression analyses between κ_a and Q (left) and κ_a and S_{25} (right). Dashed lines denote limits of $\pm 10\%$ error in estimates around forced regression line.

Table 2. Regression results between Q and κ_a, and between S_{25} and κ_a. Note that p estimates cannot be calculated for forced linear regression.

Independent variable	Dependent variable	Regular linear regression				Forced linear regression			
		slope	*intercept*	R^2	*p*	*slope*	*intercept*	R^2	*p*
Q	κ_a	-3.134	0.401	0.577	< 0.001	-3.028	0.399	0.505	-
S_{25}	κ_a	-0.681	0.396	0.746	< 0.001	-0.705	0.399	0.714	-

6. Discussion

There is substantial variability in the apparent von Kármán parameter caused by the presence of sand in the wind, and this variability leads to over-estimation of shear velocity ($u_* > u_*'$). Our results (Table 1) indicate that the mean over-estimation is about 20% for sand-laden wind and that the over estimation increases with increasing grain concentrations. The results also indicate that about 60-75% of the variation in κ_a is explained, statistically, by changes in sand transport.

There are several sources of the unexplained variance. It has been suggested [*Einstein and Chien*, 1955] that grain size asserts an influence on κ_a, so we used multiple regression to test this hypothesis. The results substantiated the primary importance of sand transport and indicated that including mean grain size increased R^2 minimally, and that increase was not statistically significant at 95% confidence. We believe that most of the unexplained variance is, instead, a result of experimental error.

There are numerous sources of error in our data, several of which we believe are important. First, we expect errors of up to about 5% in estimations of u_*', based on the assessment of *van Boxel et al.* [2004]. Such errors will propagate linearly into errors in κ_a. Second, there are errors in estimating the best-fit line for the slope of the velocity profile, m, and thus link estimates of u_*' with κ_a. We calculated the standard errors of the 15 slope estimates with sand transport. The errors averaged 5% of the slope value, increasing with decreasing R^2, to a

maximum of 9% at our R^2 cutoff of 0.985. The third source of error stems from the inherent variability of the saltation system. It has been shown that 20-25% variability in transport rates are common over distances of about a meter and time scales of 10-15 minutes [*Gares et al.*, 1996; *Jackson et al.*, 2006]. The distance across our experimental arrays, comprising the hose-trap array, cup anemometer array and ultrasonic anemometer, was less than two meters, enough that we should expect differences in transport between the trap locations and the anemometer arrays. Such errors will influence the results of the regression analysis relating κ_a to transport rates and sand concentrations, potentially accounting for individual run errors of 10% or more. Errors of these three types should manifest randomly through our data, causing much of the scatter around the regression lines. To illustrate the potential influence of these errors (or others), we have marked 10% error limits about the forced regression lines in Figure 1.

It is clear that the relationships reported in Equations 11 and 12 cannot be applied uncritically. The inverse regression functions require κ_a to become quite small, and eventually negative, as transport increases beyond the range of our experimental conditions. This indicates that the true relationships are non-linear, but of a form we cannot determine.

Finally, we emphasize that this work is not to suggest that the actual von Kármán constant is changing with sediment transport. The influence of saltating sand on the velocity profile is better described using a Monin-Obhukov and Richardson number correction that uses κ = 0.40. However, for estimations of shear velocity based on velocity profiles alone, the apparent von Kármán parameter should be used to account for the transport induced variability.

7. Conclusions

We completed a field experiment to test the hypothesis that sand transport causes an apparent change in the von Kármán constant as it is typically used to estimate shear velocity: $u_* = m\kappa$. We follow the usage of *Wright and Parker* [2004] to designate this fluctuating term "the

apparent von Kármán parameter, κ_a." For clear air flow, i.e., without saltating grains, our analysis indicated that, on average, $\kappa = \kappa_a$. For sand-laden wind, there is an inverse linear relationship between the apparent von Kármán parameter and sediment transport rates or bulk sediment concentrations. We found estimates of κ_a as low as 0.264 for our field data. Our specific conclusions are:

1. The apparent von Kármán parameter, κ_a, changes with aeolian sand transport in a manner analogous to that found for hydrodynamic systems. This is a result of decreased K and an assumption that l still scales only with z.
2. For transport conditions similar to those reported herein, changes in κ_a can be predicted using sand transport rates or bulk, gravimetric sand concentration data using the empirical regression relationships:

$$\kappa_a = -3.028Q + 0.399 \text{ or } \kappa_a = -0.705S_{25} + 0.399$$

3. Failure to adjust κ_a to account for changing transport intensity will result in over estimation of shear velocity and even greater over estimation of sand transport rates.

Most field experiments that measure aeolian sand transport rates find that predicted rates are usually much greater than measured rates [Sherman et al., 1998]. Causes of this mismatch have been the focus of much speculation, often attributed to local departures from ideal transport conditions or weaknesses in experimental design. We believe the results of this research point to another source of over prediction when shear velocity is estimated using velocity profiles: the assumption that $u_* = m\kappa$.

Acknowledgements. This study was funded by grants from the National Science Foundation, Geography and Spatial Sciences Program (#0727775 and #0822482). We are also thankful for the valuable field support from the staff of LABOMAR, University of Ceará, especially Professor Luís P. Maia, Paulo H. G. O. Sousa, Robério M. Sampaio, and Eduardo C. M. de

Borbaand. We also appreciate the valuable comments and suggestions of the four anonymous reviewers and the associate editor. This project is registered with the Brazilian Ministry of the Environment, Sistema de Autorização e Informação em Biodiversidade, Registration Number 18038-1.

References

Adams, C. E., and G. L. J. Weatherly (1981), Some effects of suspended sediment stratification on an oceanic bottom boundary layer, *J. Geophys. Res., 86*(C5), 4161-4172, doi: 10.1029/JC086iC05p04161.

Andreas, E. L., K. J. Claffey, R. E. Jordan, C. W. Fairall, P. S. Guest, P. O. G. Persson and A. A. Grachev (2006), Evaluations of the von Kármán constant in the atmospheric surface layer, *J. Fluid Mech., 559*, 117-149, doi: 10.1017/S0022112006000164.

Bagnold, R. A. (1936), The movement of desert sand, *Proc. R. Soc. London, Ser. A, 157*(892), 594-620, doi: 10.1098/rspa.1936.0218.

Bauer, B. O. (2009), Contemporary research in aeolian geomorphology, *Geomorphology, 105*(1-2), 1-5, doi: 10.1016/j.geomorph.2008.02.014.

Bennett, S. J, J. S. Bridge, J. L. Best (1998), Fluid and sediment dynamics of upper stage plane beds, *J. Geophys. Res., 103*(C1), 1239-1274, doi: 10.1029/97JC02764.

Best, J. L., S. J. Bennett, J. S. Bridge, and M. Leeder (1997), Turbulence modulation and particle velocities over flat sand beds at low transport rates, *J. Hydraul. Eng., 123*(12), 1118-1129, doi: 10.1061/(ASCE)0733-9429(1997)123:12(1118).

Dong, Z., X. Liu, H. Wang, and X. Wang (2003), Aeolian sand transport: a wind tunnel model, *Sediment. Geol., 161*(1-2), 71-83, doi: 10.1016/S0037-0738(02)00396-2.

Elata, C. and A. T. Ippen (1961), *The dynamics of open channel flow with suspensions of neutrally buoyant particles*, Techn. Rep. No. 45. Mass.Inst. of Techn. Dept. of Civil and Sanitary Engr. 69 pp.

Ellis, J. T., B. Li, E. J. Farrell, and D. J. Sherman (2009), Protocols for characterizing aeolian mass-flux profiles, *Aeolian Res., 1*(1-2), 19-26, doi: 10.1016/j.aeolia.2009.02.001.

Einstein, H. A., and N. Chien (1955), Effects of heavy sediment concentration near the bed on velocity and sediment distribution. In *Missouri River Div. Sediment Series Rep. No. 8*, University of California, Berkeley, CA.

Frenzen, P., and C. A. Vogel (1995a), A further note "on the magnitude and apparent range of variation of the von Kármán constant", *Boundary Layer Meteorol., 75*(3), 315-317, doi: 10.1007/BF00712700.

Frenzen, P., and C. A. Vogel (1995b), On the magnitude and apparent range of variation of the von Kármán constant in the atmospheric surface layer, *Boundary Layer Meteorol., 72*, 371-392, doi: 10.1007/BF00709000.

Gares, P. A., R. G. D. Davidson-Arnott, B. O. Bauer, D. J. Sherman, R. W. G. Carter, D. W. T. Jackson, and K. F. Nordstrom (1996), Alongshore variations in aeolian sediment transport: Carrick Finn Strand, Ireland, *J. Coastal Res., 12*(3), 673-682.

Glickman, T. S. (2000), *Glossary of Meteorology*, 855 pp., American Meteorology Society, Boston, Mass.

Hobbs, W. H. (1917), The erosional and degradational processes of deserts, with especial reference to the origin of desert depressions, *Ann. Assoc. Am. Geogr., 7*, 25-60, doi: 10.1080/00045601709357054.

Jackson, N. L., D. J. Sherman, P. A. Hesp, A. H. F. Klein, F. Ballasteros, and K.F. Nordstrom (2006), Small-scale spatial variations in aeolian sediment transport on a fine-sand beach, *J. Coastal Res., SI 39*, 379-383.

Keulegan, G. H.(1938), *Laws of turbulent flow in rough channels*, Res. Paper No. 1151. pp. 707-741. US Dept. of Commerce, Nat. Bureau of Standards, J. of Res. of the Nat. Bureau of Standards, Vol. 21.

Lettau, K., and H. Lettau (1977), Experimental and micrometeorological field studies of dune migration, in *Exploring the World's Driest Climate*, edited by K. Lettau and H. Lettau, pp. 110-147, Center for Climatic Research, University of Wisconsin-Madison, IES Report 101.

Liu, X., Z. Dong, and X. Wang (2006), Wind tunnel modeling and measurements of the flux of wind-blown sand, *J. Arid Environ., 66*(4), 657-672, doi: 10.1016/j.jaridenv.2005.11.010.

McKeon, B. J., J. Li, W. Jiang, J. F. Morrison and A. J. Smits (2004), Further observations on the mean velocity distribution in fully developed pipe flow, , *J. Fluid Mech., 501*, 135-147, doi: 10.1017/S0022112003007304.

Nezu, I., and R. Azuma (2004), Turbulence characteristics and interaction between particles and fluid in particle-laden open channel flows, *J. Hydraul. Eng., 130*(10), 988-1001, doi: 10.1061/(ASCE)0733-9429(2004)130:10(988).

Nikuradse, J. (1932), Gesetzmässigkeit der turbulenten Strömung in glatten Rohren, *VDI Forshungsh., 356*(B3), 1-36. (Laws of turbulent flow in smooth pipes, translated from German, *NASA TT F-10359*, 1966.).

Owen, P.R. (1964), Saltation of uniform grains in air. , *J. Fluid Mech.20*. 225–242, doi:10.1017/S0022112064001173.

Pease, P., S. Lecce, P. Gates, and M. Lange (2002), Suggestions for Low-Cost Equipment for Physical Geography II: Field Equipment, *J. Geogr., 101*(5), 199-206, doi: 10.1080/00221340208978500.

Sherman, D. J., and E. J. Farrell (2008), Aerodynamic roughness lengths over movable beds: Comparison of wind tunnel and field data, *J. Geophys. Res.*, 113, F02S08, doi:10.1029/2007JF000784.

Sherman, D. J., D. W. T. Jackson, S. L. Namikas, and J. Wang (1998), Wind-blown sand on beaches: an evaluation of models, *Geomorphology, 22*(2), 113-133, doi: 10.1016/S0169-555X(97)00062-7.

Smith, J. D., and S. R. McLean (1977), Spatially averaged flow over a wavy surface, *J. Geophys. Res., 82*(12), 1735-1746, doi: 10.1029/JC082i012p01735.

Sørensen, M. (2004), On the rate of aeolian sand transport, *Geomorphology, 59*(1-4), 53-62, doi: 10.1016/j.geomorph.2003.09.005.

Van Boxel, J. H., G. Sterk, and S. M. Arens (2004), Sonic anemometers in aeolian sediment transport research, *Geomorphology, 59*(1), 131-147, doi: 10.1016/j.geomorph.2003.09.011.

Vanoni, V. A., and G. N. Nomicos (1960), Resistant properties of sediment-laden streams, *Trans. Am. Soc. Civ. Eng., 125*, 1140-1175.

Wippermann, F. K., and G. Gross (1986), The wind-induced shaping and migration of an isolated dune: a numerical experiment, *Boundary Layer Meteorol., 36*(4), 319-334, doi: 10.1007/BF00118335.

Wright, S., and G. Parker (2004), Density stratification effects in sand-bed rivers, *J. Hydraul. Eng., 130*(8), 783-795, doi: 10.1061/(ASCE)0733-9429(2004)130:8(783).

VITA

Name:	Bailiang Li
Address:	Department of Geography, Texas A&M University, TX 77843-3147
Email Address:	libl@tamu.edu
Education:	B.S., Natural Resources and Environmental Ecology, Peking University, 2000
	M.S., Cartography and Geographical Information System, Chinese Academy of Sciences, 2003
	Ph.D., Geography, Texas A&M University, 2010